Critical fluctuations and molecular dynamics at liquid-crystalline phase transitions. II. Electron spin resonance experiments

Akbar Nayeem, S. B. Rananavare,[a] V. S. S. Sastry,[b] and Jack H. Freed

Baker Laboratory of Chemistry, Cornell University, Ithaca, New York 14853-1301

Electron spin resonance (ESR) relaxation studies at nematic–isotropic (N–I), and nematic–smectic-A (N–S_A) phase transitions in two liquid crystals, 4O,6 and 6OCB–8OCB, using the three spin probes, PD-tempone, MOTA, and P are described. In general, one finds that (i) at the N–I transition, as T_{NI} is approached, the linewidths diverge with a critical exponent of 1/2; (ii) at the N–S_A transition, the linewidths diverge with a 1/3 power law as the transition is approached from the nematic side. The nature of the critical divergences in the relaxation parameters is interpreted and analyzed in terms of fluctuations in the nematic and smectic order parameters at the respective transitions and the coupling of the orientational dynamics of the probe to these modes. Good quantitative agreement with theory for the N–I transition required the inclusion of the effects of asymmetric probe ordering. The theory developed in detail in paper I is applied to interpret the results at the N–S_A transition. This theory is extended to include the effects of the measured anisotropies in (a) translational diffusion of the probe, (b) smectic correlation lengths, and (c) dynamic scaling exponents. In general, the magnitudes of the observed effects as well as their critical exponents are of the order expected, provided the averaging of the effects of density fluctuations within a smectic layer by probe diffusion is incomplete as a result of hindered diffusion.

I. INTRODUCTION

Liquid crystals exhibit a wide variety of ordered phases,[1,2] including transitions between phases differing from each other in their degree of order and symmetry.[3] Several experimental methods, which include light scattering,[4,5] NMR,[6–8] x-ray diffraction,[9–12] and adiabatic calorimetry[3,10,13–15] (each of which is sensitive to some characteristic property of the liquid crystal), have been used to study mesomorphic transitions. Such transitions are typically heralded by characteristic pretransitional effects (e.g., divergences in heat capacities, viscosities, elastic constants, correlation lengths) that can often provide insight into the nature of the transition.

Pretransitional effects which are manifested as "critical anomalies" in magnetic-resonance relaxation measurements, are caused by fluctuations in the order parameter appropriate to the particular transition.[16–18] Thus, for example, although the long-range order vanishes abruptly when warming to the nematic–isotropic (N–I) transition, there is considerable evidence to indicate that a short-range order analogous to the nematic order persists in the isotropic phase just above the transition.[4] Similarly, in liquid crystals exhibiting an underlying smectic-A (S_A) phase, at temperatures just above T_{NA}, the N–S_A transition, there are small domains of cybotactic clusters, i.e., regions with local smectic order, and as T–T_{NA} approaches zero (with $T > T_{NA}$), the regions of local smectic order grow.[2,19] Also, since the symmetry of the smectic phase requires twist and bend deformations to

become forbidden, the associated elastic constants must diverge as the S_A phase is approached from above.

The fluctuations in the order parameter(s) that occur at the phase transitions can result in a slowly fluctuating orientational potential at the site of the probe molecule, thus modulating the rotational reorientation of the probe. Such modulations have been shown to lead to anomalous effects in spin relaxation, manifested as critical-type divergences for the hyperfine lines.[16,20] Detailed studies of electron-spin relaxation and orientational ordering at liquid-crystalline phase transitions using a variety of spin probes therefore provides important complementary information to that obtained using the more traditional techniques, shedding light on the subtle molecular features that characterize these transitions, which are typically second order or weakly first order. The nature of the linewidth divergences at these transitions can also be useful in addressing how the molecular dynamics of the spin probe couples to the collective modes. The critical exponents describing the divergence in the relaxation rates provide a useful indication of the nature of this coupling.[17,21]

In this work, we describe electron-spin-relaxation studies of the N–I, N–S_A, and S_A–RN (reentrant nematic) phase transitions, and analyze them in the context of the models developed in paper I (Ref. 21) and previously.[17] These studies were performed using three nitroxide spin probes, perdeuterated 2,2',6,6' tetramethyl 4-piperidine 1-oxyl (PD-tempone), partially deuterated 4-methyl amino 2,2',6,6' tetramethyl piperidine 1-oxyl (MOTA), and partially deuterated 2,2',6,6' tetramethyl 4-(butyloxy) benzylamino piperidine 1-oxyl (P-probe) (Fig. 1), dissolved in two liquid crystals. These are (i) 4 n-butoxy benzylidene 4' n-hexyl aniline (4O,6), which exhibits the transitions I–N–S_A–S_B–

Acronym	Name	Structure
PD-Tempone	2,2′,6,6′-tetramethyl-4-piperidine N-oxide (perdeuterated)	
MOTA	4-methylamino-2,2′,6,6′-tetramethyl-piperidinyl-N-oxide (perdeuterated ring)	
P	2,2′,6,6′-tetramethyl-4-(butyloxy)-benzoylamino-piperidine N-oxide (perdeuterated piperidine ring)	
CSL	3′,3′-dimethyloxazolidinyl-N-oxy 2′,3 − 5α-cholestane	

FIG. 1. Structures of some nitroxide spin probes.

K, and (ii) a binary mixture containing 27% *n*-hexyloxy cyanobiphenyl (6OCB) in *n*-octyloxy cyanobiphenyl (8OCB), a system that exhibits a reentrant nematic phase (I–N–S_A–N).[22,23] The structures of these liquid crystals are shown in Fig. 2 along with their phase-transition temperatures.

The linewidth parameters related to spin relaxation were studied as a function of temperature, placing special emphasis on the regions at the vicinity of the phase transitions. For this purpose, a temperature controller with millikelvin resolution was employed, and data were collected at 10–20 mK intervals near the transition. The critical contributions to the relaxation parameters are analyzed in terms of a power law in temperature, $k(T - T^*)^\gamma$, where T^* denotes the transition temperature and γ is a critical exponent describing the divergence of the linewidths. The latter is discussed in the context of the proposed models of molecular dynamics at the mesomorphic transitions.

The experimental details are given in Sec. II. Section III reviews the theoretical background, and provides a discussion of current models relevant to our results, while Sec. IV describes the methods of data treatment and analysis. The results and interpretation are given in Sec. V. The conclusions appear in Sec. VI. Finally, Appendix A describes the effects of anisotropy of ordering of the probe molecule on the spectral densities associated with the N–I transition; Appendixes B and C provide a more general formulation of the spectral density for the N–S_A transition, allowing for anisotropy in the coherence lengths describing the N–S_A transition; and Appendix D presents a simple analysis of the effects of nematic order-parameter fluctuations at the N–S_A transition.

ACRONYM	NAME	FORMULA
6OCB	4-cyano 4′-n-hexyloxybiphenyl	NC-Φ-Φ-OC$_6$H$_{13}$
8OCB	4-cyano 4′-n-octyloxybiphenyl	NC-Φ-Φ-OC$_8$H$_{17}$
4O,6	N-(p-butoxybenzylidene)-p-n-hexylaniline	H$_9$C$_4$O-Φ-CH=N-Φ-C$_6$H$_{13}$
4O,7	N-(p-butoxybenzylidene)-p-n-heptylaniline	H$_9$C$_4$O-Φ-CH=N-Φ-C$_7$H$_{15}$
8CB	4-cyano 4′-n-octylbiphenyl	NC-Φ-Φ-C$_8$H$_{17}$

Transition temperatures of some liquid crystals[*]

a) 27% 6OCB – 73% 8OCB	K (24°C) N (31°C) S$_A$ (45°C) N (79°C) I
b) 8CB	K (21°C) S$_A$ (34°C) N (41°C) I
c) 4O,6	K (18°C) S$_B$ (48°C) S$_A$ (55°C) N (78°C) I
d) 4O,7	K (49°C) S$_C$ (50°C) S$_A$ (56°C) N (81°C) I

*References: a) Ref. 23; b) G.W. Gray, J. Phys. (Paris) C-36, 337 (1975); c) G.W. Smith and Z.G. Gardlund, J. Chem. Phys. 59, 3214 (1973); d) Ref. 10.

FIG. 2. Structures of some liquid crystals.

II. EXPERIMENT

A. Preparation of samples

The liquid crystals 4-*n*-hexyloxy 4′ cyano biphenyl (6OCB) and 4-*n*-octyloxy-4′-cyano biphenyl (8OCB) were

purchased from BDH Chemicals Ltd. Since their phase-transition temperatures agreed with the published values, these compounds were used without further purification. The eutectic mixture of 27 wt. % 6OCB in 8OCB was prepared by weighing the two components ($\pm$ 0.1% precision) and heating them together till the clearing point, followed by rapid stirring to ensure uniform mixing. The composition of this mixture was also verified by comparing its phase-transition temperatures with the phase diagram for the 6OCB–8OCB system.[23] N-(4-butoxy benzylidene) 4′ n-hexyl aniline (4O,6) was prepared by Dr. E. Igner by condensing equimolar quantities of 4-n-butoxybenzaldehyde (obtained from Eastman Kodak Chemicals) and 4-n-hexylaniline (from Frinton Laboratories) in absolute ethanol followed by recrystallization from the same solvent. The transition temperatures of these liquid crystals are shown in Fig. 2.

The three nitroxide spin probes used in this study, PD-tempone, MOTA, and P-probe all contained a deuterated piperidine ring in order to minimize line broadening due to proton superhyperfine structure. PD-tempone was prepared by Dr. Eva Igner, while MOTA and P-probe were synthesized by Professor J. Pilar and Dr. Sidney Wolfe, respectively. The structures of these radicals are shown in Fig. 1.

Solutions of spin probe in the liquid-crystal solvents were typically 0.4 to 0.5 mM in concentration. Once prepared, these solutions were transferred to a Pyrex sample holder containing sidearms, which were glass capillaries about 0.9 mm in diameter. Following freeze–pump–thaw degassing on a vacuum line, the solutions were transferred to the capillary sidearms, where they were sealed under a pressure below 0.1 mTorr.

B. ESR spectrometer and helix system

All data were recorded at X-band frequencies on a Varian E-12 spectrometer using 25 kHz field modulation. In order to minimize line-shape distortions, the modulation amplitude was maintained at a value below one-tenth the linewidth, and the microwave power well below the saturation limit. The on-line collection and analysis of data was achieved through an interface to a Prime 850 time-shared computer, for which interactive software was developed.

The experiments described here were carried out in a thermostated Be–Cu vessel containing a slow-wave helix,[24,25] whose width was chosen in a way such that the capillary containing the sample fits snugly into it. The helix, thus also serving as the "sample holder," was surrounded by a pair of modulation coils mounted on a Teflon modulation capsule. Owing to the difficulty in tuning the helix (the line shapes were often asymmetric), the helix system required tuning at each temperature. Such tuning was achieved using a slide-screw tuner that controlled the coupling of the microwaves to the helix, and by adjusting the phase on the reference arm. The criterion for acceptable tuning was chosen to be one that symmetrized the central electron-spin-resonance (ESR) line, since it is usually the outer two lines that are most sensitive to asymmetry changes near the phase transitions (see later).

C. Temperature measurements

The fine temperature resolution (5–10 mK) was obtained using a 122 Precision Temperature controller in conjunction with a Tamson unit; the details are provided elsewhere.[25] The temperatures at the sample were measured in terms of the resistance of platinum, whose resistance as a function of temperature is accurately known. A Keithley Digital Multimeter, which could record changes in resistance of $\pm$ 1 mΩ (or temperature changes of $\pm$ 2.5 mK), was used for measuring resistances. In order to detect and determine any gradients in temperature along the length of the sample, two platinum resistors were used, and were placed at the top and at the bottom of the sample. Longitudinal gradients thus measured were on the order of 10 mK. Furthermore, any drifts in the temperature with time could also be recorded directly by the multimeter. A period of 1 h was usually sufficient to allow for temperature equilibration; temperature drifts during this period were typically 5 to 10 mK at temperatures higher than 60 °C, but increased to about 20 to 30 mK at ambient temperatures.

D. Director alignment

Measurements in the smectic phases of the liquid crystals required alignment of the director. In the nematic phase, the nematic director follows the magnetic field (~ 3.3 kG), whereas in the smectic state a magnetic field of 3.3 kG is insufficient to align the director owing to the weaker anchoring in the S_A phase.[2,26] Proper alignment in the S_A phase therefore required the use of increased magnetic fields (12 kG). Alignment was achieved by slowly cooling and heating (a few times) about T_{NA} at the rate of about 1 °C per hour, and finally cooling into the well-formed S_A phase (4 to 5 °C below T_{NA}).[26,27] Linewidth data at the N side of T_{NA} were collected upon cooling, whereas those at the S_A side were collected upon heating from the well-formed S_A phase. As T_{NA} is approached, the hyperfine line shapes become asymmetric because of critical effects on the director alignment, a matter discussed in Sec. V B 5. Thus, in order to avoid such problems from corrupting the measured linewidths, we only used data over the temperature ranges where the lines were very nearly symmetric. Typical values (e.g., PD-tempone in 6OCB–8OCB) were $T - T_{NA} > 0.1$ °C [corresponding to $t \equiv (T - T_{NA})/T_{NA} = 3 \times 10^{-4}$] above T_{NA}, and $T - T_{NA} < -0.3$ °C ($t = 9 \times 10^{-4}$) below T_{NA}.

By first rotating the director to be perpendicular to the magnetic field deep into the S_A phase, and then raising the temperature to be near T_{NA}, the line-shape distortions are dramatically enhanced. This was the method whereby we located T_{NA} approximately, before initiating a detailed study on a given sample.

E. Spectral measurements

The hyperfine splittings were measured with respect to those from PD-tempone in toluene-d_8, taken as the primary standard for calibration. The linewidths were calibrated with respect to spectra from potassium tetracyanoethylene [K$^+$(TCNE)$^-$] in dimethylethylene (DME). In both

cases, computer software written by Dr. S. A. Zager was used to control the rate of data acquisition and then convert the (amplified) recorded signal voltages to digital form.[25]

The intrinsic linewidths for each of the three hyperfine lines were obtained by fitting each line to a superposition of Lorentzian lines separated by a_D, the deuterium coupling constant. Thus, each ^{14}N hyperfine line was simulated by calculating the envelope of superhyperfine lines due to the dipolar coupling of the electron spin to the neighboring 12 methyl deuterons, all assumed to possess the same coupling constant a_D.[27,28] The coupling of the electron spin to the ring deuterons is known to be much smaller and was therefore neglected. The computer program used for these calculations also had the feature of taking into account the asymmetry of the lines. Asymmetric lines were treated as linear combinations of absorption and dispersion components,[29] and the program generated the proper admixture of each of these for each intrinsic width.

III. TREATMENT OF DATA

The experimental ESR derivative linewidths δ (in G) were corrected for deuterium inhomogeneous broadening as described above, and were then fitted to the expression

$$\delta(M_I) = A + BM_I + CM_I^2, \qquad (1)$$

where M_I is the z component of the ^{14}N nuclear-spin quantum number.[30] The parameters A, B, and C are directly related to the tumbling motion of the spin probe. Our results for B and C with temperature are shown in Figs. 3(a) and 3(b) for 4O,6 and 6OCB–8OCB, respectively. It is clear from these figures that the values of B and C at the phase transitions are anomalous in the sense that they appear to diverge as T^*, the phase-transition temperature, is approached from either one or both sides of the transition.

The anomalous contributions to B and C (B_{anom} and C_{anom}) must be obtained by subtracting out the main contributions to B and C (B_0 and C_0), i.e., those that arise due to rotational motions which constitute the only contribution away from T^*. In those cases, where the order parameter did not change much with temperature (e.g., near the N–S_A transition, or at the isotropic side of the N–I transition) a five-parameter fit was performed, using a nonlinear least-squares routine based on the Marquardt algorithm,[31,32] to yield values of k, T^*, and σ. We employed an expression of the form

$$B,C = k(T - T^*)^\sigma + c \exp(-b/T), \qquad (2)$$

where the second term on the right models the temperature variation of the secular spectral densities arising from simple rotational diffusion which dominate B_0 and C_0, and the first term models B_{anom} or C_{anom} (cf. Sec. IV). That is,

$$B_{anom}, C_{anom} = k(T - T^*)^\sigma. \qquad (3)$$

On the nematic side of the N–I transition, the probe order parameter is a significant function of temperature, so B_0 and C_0 have a more complicated temperature dependence than given in Eq. (2). Thus we first estimated B_0 and C_0 as fol-

lows, and then used Eq. (3) to fit the residual B_0 and C_0. In regions away from T^*, where B_{anom} and C_{anom} are negligible, the linewidth parameters B and C were compared to values of B_0 and C_0 that were calculated using a range of values of $\tau_{\bar{R}}$ and N [given that $R_\perp$ and $R_\parallel$ are the perpendicular and parallel components of the rotational diffusion tensor, then $\tau_{\bar{R}}^{-1} \equiv 6(R_\perp R_\parallel)^{1/2}$ and $N \equiv R_\parallel/R_\perp$]. The probe order parameter S ($S \equiv \langle 3\cos^2\theta - 1\rangle/2$, where θ is the angle that the ordering axis of the spin probe makes with the mean director), which was also needed for the calculation, was obtained in the standard fashion from the observed hyperfine splittings.[22,27] The magnetic parameters for the different systems studied here are shown in Table I. From such comparisons, the values of $\tau_{\bar{R}}$ and N that best represented the experimental data were selected. In order to obtain $\tau_{\bar{R}}$ at the critical regions, a linear extrapolation of $\ln \tau_{\bar{R}}$ vs $1/T$ was performed. From a knowledge of the order parameters near T^* obtained from the hyperfine splittings,[22,27] and the extrapolated values of $\tau_{\bar{R}}$ and N, B_0 and C_0 were calculated. B_{anom} and C_{anom} were obtained by subtracting B_0 and C_0 from the experimental values of B and C, respectively.

The analysis also provided the uncertainties in the values of the parameters associated with the fits to the data, as shown in Tables I and II.

In the case of MOTA in 6OCB–8OCB, the linewidth data near both the N–I and N–S_A transitions showed little, if any, signs of critical divergence when compared with similar data for PD-tempone in 6OCB–8OCB, even though a five-parameter fit to these data successfully gave exponents and transition temperatures that were compatible with the latter. A more objective criterion (than visual comparison) was thus needed in order to better discern whether a five-parameter fit, i.e., Eq. (2) [or Eq. (3) when appropriate] was warranted rather than a two-parameter fit that represented the Arrhenius contribution alone, i.e., the second term in Eq. (2). This was also desirable in discerning critical effects at transitions where they were weak, e.g., the N–S_A transitions. For this purpose of comparing the two nested models, the F ratio of the partial (two-parameter) to the full (five-parameter) model was used to calculate the probability for the Fisher F function $P(\nu_e,\nu_f;F)$ (where $\nu_e \equiv P_f - P_p$, $\nu_f \equiv N - P_f$, and F is the F ratio defined as the ratio of the reduced χ^2's for the two models: $F \equiv [(\chi_P^2 - \chi_F^2)/\nu_e]/(\chi_F^2/\nu_F)$; here N is the number of data points to be fitted, P_f and P_p are the number of parameters for the full and partial models (five and two in our case), and χ_P^2, χ_F^2 are the values of χ^2 for the partial and full parameter fits, respectively).[31,32] $P(\nu_e,\nu_f;F)$ provides a quantitative statistical measure of the necessity for performing a five-parameter as compared to a two-parameter fit. In some cases, we also compared the two- and five-parameter fits with a three-parameter fit wherein we fixed T^* and σ at the values from the five-parameter fit, allowing only b, c, and k to vary, in order to satisfy ourselves that the full model was not, in fact, redundant.
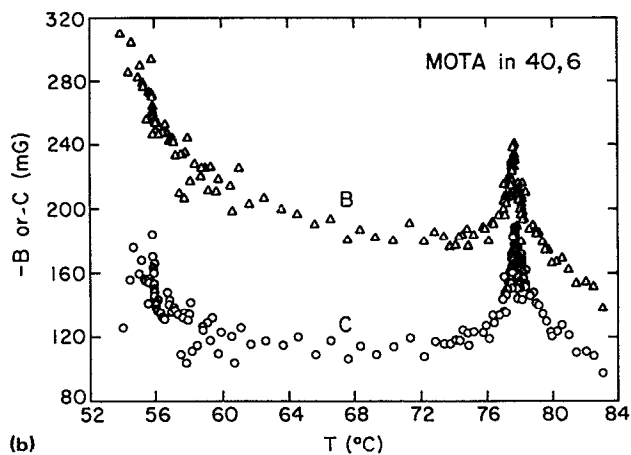
The results of comparing the two- vs five-parameter fits are also summarized in Tables II and III, which show the $P(\nu_e,\nu_f;F)$ as percent confidence level for the five-parameter fits that were obtained in the various cases for the nonlinear
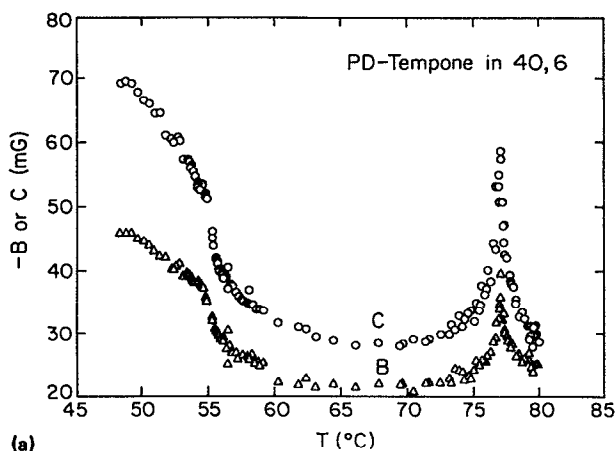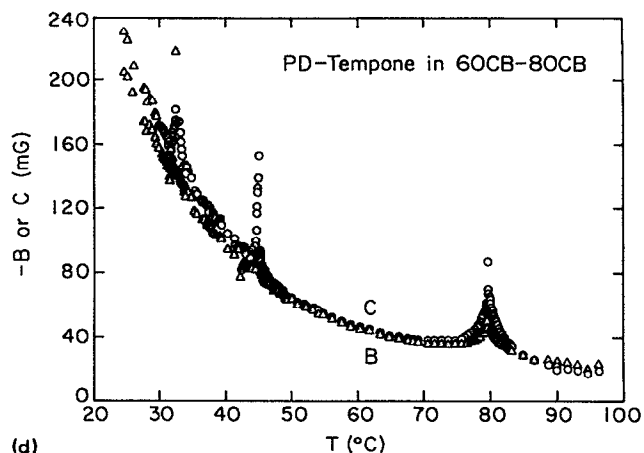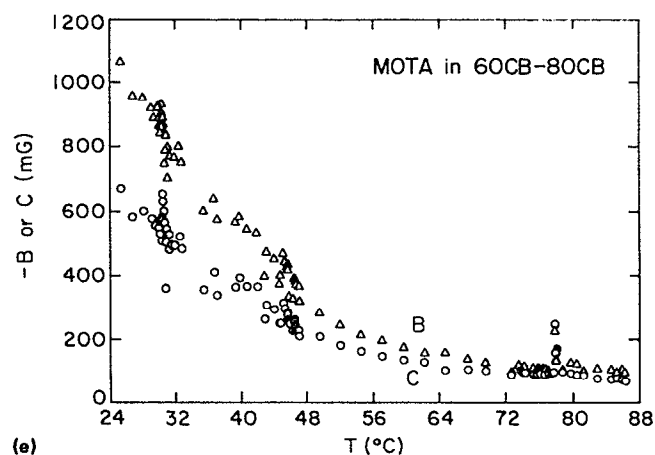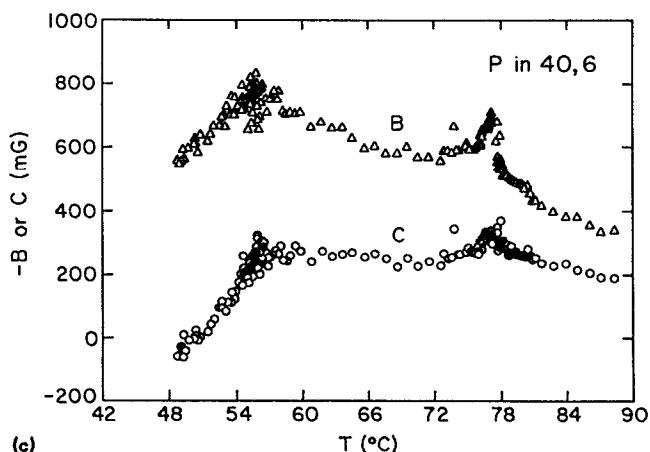
FIG. 3. Temperature variation of linewidth parameters B and C for (a) PD–tempone, (b) MOTA, and (c) P in 4O,6, and (d) PD–tempone and (e) MOTA in 6OCB–8OCB.

least-squares fits to the B and C data. In those cases where the critical divergence was dramatic enough (typically the N–I transitions), the F test became redundant, since the two-parameter fit did not even converge for the data. The results showed that, at the N–I transition, all cases but one were significantly in favor of the five-parameter model (which we took as a 96% confidence level or better), with the probability being highest for PD-tempone and decreasing with in-

creasing probe size. In the one case of MOTA in 6OCB–8OCB the differences between the two- vs five-parameter models were not unequivocally in favor of the latter (i.e., 86% on the isotropic side of the N–I transition and no observed divergence on the nematic side). The results for the N–S_A transition also showed that the five-parameter model was favored by a 96% probability or better, except for the B data at the S_A side of the S_A–RN transition for PD-tempone

TABLE I. Magnetic parameters for spin probes in 4O,6 and 6OCB–8OCB.

Probe	Solvent	$g_{x'}$	$g_{y'}$	$g_{z'}$	$A_{x'}$ (G)	$A_{y'}$ (G)	$A_{z'}$ (G)
PD–tempone	6OCB–8OCB	2.0099	2.0062	2.00215	5.60	5.00	33.65
MOTA	6OCB–8OCB	2.0099	2.0064	2.0023	5.92	5.29	35.60
PD–tempone	4O,6	2.0099	2.0062	2.00215	5.57	4.98	33.49
MOTA	4O,6	2.0099	2.0064	2.0023	5.89	5.26	35.41
P–probe	4O,6	2.0094	2.0058	2.0026	7.32	7.82	31.50

in 6OCB–8OCB (71%) (and again for the anomalous case of MOTA in 6OCB–8OCB). This provides the clear justification for including the critical term in the analysis.

IV. THEORETICAL BACKGROUND

In liquid-crystalline systems, Freed[17] has shown that the molecular dynamics of spin-bearing probe molecules can be described in terms of a composite Markov process consisting of the (faster) rotational reorientational motion of the radicals and the (slower) director or order-parameter fluctuations. When the fluctuations are included in lowest order, the analysis leads to the result that the spectral densities for spin relaxation can be decomposed into a sum of three terms: (i) rotational reorientation of the molecule in the equilibrium potential of mean torque, (ii) the effect of order-director and/or order-parameter fluctuations, and (iii) a small negative cross term between processes (i) and (ii) (in the case of the *N–I* transition) which bears a simple relation to (ii). In regions away from criticality, the contribution from (ii),

which involves the coupling of the molecular dynamics to the collective modes (which occur on a longer time scale than the probe reorientational motions), is often small compared to (i). However, (ii) plays a significant role in influencing spin relaxation at the vicinity of mesophase transitions. The increased contribution from (ii) is caused by divergences in correlation lengths accompanying the buildup of the appropriate order parameter for the given transition as well as the associated critical slowing down of the relaxation of these collective modes. Thus, at the *I–N* transition, which is accompanied by a growth in orientational order, fluctuations in the orientational order parameter cause divergences in the correlation lengths as the transition is approached. Similarly, at the *N–S_A* transition, the growth of positional order causes fluctuations in the mass density which also cause the correlation lengths to diverge (but at a different rate with temperature than for *N–I* because of fluctuations in a different kind of order parameter and phase transition). It is the nature of the temperature variations of the correlation lengths and the slowing down of the collec-

TABLE II. Nonlinear least-squares analysis of ESR linewidth parameters B, C (mG) $= k(T - T^*)^\sigma + ce^{-b/T}$ at $N \leftrightarrow I$ transition.[a]

System	Phase	B or C	k	T^* (°C)	σ	c (mG)	b (K)	$P_F(\nu_1, \nu_2; F)$
PDT/6OCB–8OCB	*I*	*B*	14.2 ± 1.9	79.43 ± 0.09	− 0.43 ± 0.09	$(1.6 \pm 0.1) \times 10^{-3}$	3425 ± 27	> 99.99
		C	46.4 ± 2.2	79.27 ± 0.05	− 0.40 ± 0.03	$(1.5 \pm 0.3) \times 10^{-3}$	3064 ± 89	b
	N[c]	*B*	16.20 ± 0.03	79.93 ± 0.02	− 0.50 ± 0.01	···	···	b
		C	29.90 ± 0.03	80.02 ± 0.01	− 0.56 ± 0.01	···	···	b
PDT/4O,6[c,d]	*I*	*B*	7.6 ± 1.7	76.7 ± 0.2	− 0.49 ± 0.11	···	···	> 99.99
		C	17.4 ± 2.1	77.0 ± 0.2	− 0.45 ± 0.09	···	···	> 99.99
	N	*B*	4.46 ± 0.05	77.17 ± 0.02	− 0.48 ± 0.01	···	···	b
		C	9.7 ± 0.2	77.24 ± 0.01	− 0.54 ± 0.02	···	···	> 99.99
MOTA/6OCB–8OCB	*I*	*B*	42.0 ± 4.9	78.5 ± 0.5	− 0.48 ± 0.08	$(4.1 \pm 0.2) \times 10^{-4}$	4375 ± 15	85.99
		C	39.0 ± 15.7	78.3 ± 1.0	− 0.48 ± 0.04	$(1.6 \pm 0.3) \times 10^{-4}$	4564 ± 63	87.00
	N[c]		···	···	···	···	···	···
MOTA/4O,6	*I*	*B*	58.4 ± 5.4	77.2 ± 0.1	− 0.47 ± 0.02	$(3.2 \pm 0.1) \times 10^{-3}$	3755 ± 14	> 99.99
		C	68.3 ± 5.7	77.2 ± 0.1	− 0.50 ± 0.02	$(2.5 \pm 0.2) \times 10^{-3}$	3688 ± 23	> 99.99
	N[c]	*B*	43.0 ± 0.2	77.90 ± 0.02	− 0.48 ± 0.01	···	···	b
		C	44.0 ± 0.2	77.93 ± 0.03	− 0.50 ± 0.01	···	···	b
P/4O,6	*I*	*B*	160.7 ± 49.1	76.6 ± 0.2	− 0.49 ± 0.12	$(3.2 \pm 0.4) \times 10^{-3}$	4126 ± 41	99.98
		C	66.3 ± 37.3	76.9 ± 0.1	− 0.50 ± 0.15	$(5.3 \pm 0.9) \times 10^{-3}$	3763 ± 62	20.0
	N[c]	*B*	209.8 ± 1.0	77.71 ± 0.01	− 0.51 ± 0.01	···	···	b
		C	125.4 ± 1.5	77.77 ± 0.03	− 0.49 ± 0.02	···	···	b

[a] B, C (mG) $= k(T - T^*)^\sigma$ in the nematic phase.
[b] Large critical effect at *N–I* transition; two-parameter fit does not converge.
[c] Three-parameter fit after subtracting nondivergent contributions.
[d] Original data from Ref. 20.
[e] No divergence in B or C observed.

TABLE III. Nonlinear least-squares analysis of ESR linewidth parameters B,C (mG) $= k(T - T^*)^\sigma + ce^{-b/T}$ at $N \leftrightarrow S_A$ transition.

System	Phase	B or C	k	T^* (°C)	σ	c (mG)	b (K)	$P_F(\nu_1,\nu_2;F)$
PDT/6OCB–8OCB[a]	N	B	16.8 ± 2.7	43.93 ± 0.03	-0.30 ± 0.02	$(3.3 \pm 0.2) \times 10^{-4}$	3847 ± 14	> 99.99
		C	12.5 ± 1.2	44.97 ± 0.01	-0.36 ± 0.03	$(1.8 \pm 0.2) \times 10^{-4}$	4079 ± 38	> 99.99
	S_A[b]	B	19.2 ± 2.7	32.75 ± 0.01	-0.33 ± 0.02	$(2.5 \pm 0.1) \times 10^{-3}$	3281 ± 8	70.95
		C	32.4 ± 3.0	32.74 ± 0.01	-0.38 ± 0.02	$(2.5 \pm 0.1) \times 10^{-3}$	3289 ± 8	99.99
PDT/4O,6[a,c]	N	B	4.1 ± 1.7	55.21 ± 0.03	-0.33 ± 0.07	$(7.0 \pm 0.6) \times 10^{-4}$	3448 ± 28	> 99.99
		C	6.0 ± 0.8	55.15 ± 0.04	-0.38 ± 0.06	$(9.9 \pm 0.3) \times 10^{-4}$	3428 ± 9	[d]
MOTA/6OCB–8OCB[a]	N	B	74.6 ± 8.5	45.4 ± 0.5	-0.37 ± 0.02	$(7.1 \pm 0.2) \times 10^{-4}$	4186 ± 7	[d]
		C	76.8 ± 6.3	44.7 ± 0.3	-0.35 ± 0.02	$(18.2 \pm 0.6) \times 10^{-4}$	3676 ± 10	[d]
	S_A[b]	B	207.3 ± 9.6	30.45 ± 0.01	-0.13 ± 0.01	$(1.2 \pm 0.1) \times 10^{-3}$	3977 ± 45	[d]
		C	262.3 ± 32.7	30.49 ± 0.01	-0.13 ± 0.02	$(1.1 \pm 0.2) \times 10^{-3}$	3727 ± 61	[d]
MOTA/4O,6[a]	N	B	8.0 ± 0.2	55.89 ± 0.01	-0.32 ± 0.01	$(1.33 \pm 0.04) \times 10^{-2}$	3225 ± 9	99.89
		C	5.2 ± 0.4	55.97 ± 0.02	-0.33 ± 0.02	$(4.6 \pm 0.2) \times 10^{-3}$	3379 ± 2	99.27
P/4O,6[c]	S_A	B	713.3 ± 2.9	56.84 ± 0.40	-0.21 ± 0.03	$(1.1 \pm 0.2) \times 10^{-3}$	3856 ± 6	99.97
		C	702.8 ± 0.7	56.96 ± 0.01	-0.23 ± 0.02	$-(3.0 \pm 0.4) \times 10^{-3}$	3858 ± 10	> 99.99

[a] No critical divergence at $S_A \to N$ transition.
[b] S_A–RN transition.
[c] Original data from Ref. 20.
[d] The χ^2 values were comparable for the two- and five-parameter fits.
[e] No critical divergence at $N \to S_A$ transition.

tive modes of reorientation that determine the "anomalous" behavior of spin relaxation at the vicinity of the phase transitions.

The temperature dependence of the spectral densities $J(\omega)$ for the linewidth parameters B and C is therefore treated as the sum of two terms:

$$J(\omega) = J^{RR}(\omega) + J^{OPF}(\omega). \tag{4}$$

The first, $J^{RR}(\omega)$, describes the rotational reorientational contribution to linewidth. In the isotropic phase, it is proportional to $\tau_R/(1 + \omega^2\tau_R^2)$, where τ_R is the rotational correlation time of the spin probe.[33] τ_R is assumed to obey an Arrhenius-like temperature law, $\tau_R \propto \exp(-E_a/RT)$, where E_a is the activation energy for reorientation. The second term, $J^{OPF}(\omega)$, denotes the contribution due to order-parameter fluctuations as discussed above. It has been noted[16] that the main contributions to B and C come from the secular and pseudosecular spectral densities, $J(0)$ and $J(\omega_a)$ [only $J(0)$ in the case of B]. $J^{OPF}(0)$ can be shown to be related to some power of the correlation length (ξ) for order fluctuations, the exponent depending on the nature of the transition and the precise model for the coupling of the molecular dynamics. The temperature dependence of $J^{OPF}(0)$ therefore depends on how ξ varies with temperature. Since this latter temperature dependence is also empirically noted to be a power law, it follows that $J^{OPF}(0) \sim (T - T^*)^\sigma$, where σ is a critical exponent. From these considerations we have

$$J^{RR}(0) \sim c \exp(-E_a/RT) \tag{5}$$

and

$$J^{OPF}(0) \sim k(T - T^*)^\sigma. \tag{6}$$

Combining Eqs. (4)–(6) gives

$$J(0) \sim c \exp(-E_a/RT) + k(T - T^*)^\sigma, \tag{7}$$

which is a relatively simple expression that was used in the previous section [cf. Eq. (2)] to simulate the linewidth behavior as a function of temperature.

In summary, the first term on the right-hand side of Eq. (7) depends on temperature, and (in the case of mesophases) the order parameter, which varies with temperature. It describes the "background" contribution to spin relaxation at the phase transitions, and it arises from reorientational motion of the spin probe in the ordering potential of the liquid-crystal molecules. The second term, $k(T - T^*)^\sigma$, describes the coupling of the molecular dynamics of the probe to the hydrodynamic modes in the liquid crystal.[17,34] The exponent σ depends on the nature of the transition (first or second order, N–I, or N–S_A). We discuss below the models for the N–I and N–S_A transitions that provide an interpretation for σ.

A. N–I transition

The orientation-dependent part of the spin Hamiltonian $\hat{\mathcal{H}}_1(\Omega)$ can be written as

$$\hat{\mathcal{H}}_1(\Omega) = \sum_{\mu,i} \sum_{L,M,K} (-1)^K F_{\mu,i}'^{(L,-K)} \mathcal{D}_{M,-K}^L(\Omega) A_{\mu,i}^{(L,M)}, \tag{8}$$

where Ω specifies the orientation of the molecular axis system relative to the lab frame defined by the static magnetic field. $\mathcal{D}_{M,-K}^L(\Omega)$ are the Wigner rotation matrix elements; the irreducible spin and molecular tensor elements, $A_{\mu,i}^{(L,M)}$ and $F_{\mu,i}'^{(L,-K)}$ respectively, are defined elsewhere.[17,27,28] The typical terms in Eq. (8) require $L = 2$. The introduction of a director frame into the Hamiltonian requires the use of two further transformations with the following sets of Euler angles:[17] (i) the angles Ψ, specifying the orientation of the mean director $\hat{n}_0(r)$ with respect to the lab frame; (ii) the

angles Ξ, specifying the instantaneous orientation of the director $[\hat{n}(r,t)]$ relative to the mean director. As a result of the combined reorientational motion and the fluctuating director (which influences the reorientational motion) $\mathcal{H}_1(\Omega)$ will be partially averaged, and its average value is given by

$$\langle \hat{\mathcal{H}}_1(\Xi) \rangle = \sum_\mu \sum_K \sum_M (-1)^K \langle \mathcal{D}^2_{M,-K}(\Omega) \rangle F_\mu'^{2,K} A_\mu^{2,M}, \tag{9}$$

where

$$\langle \mathcal{D}^2_{MK}(\Omega) \rangle = \int d\Omega\, P_{eq}(\Omega,\Xi) \mathcal{D}^2_{MK}(\Omega). \tag{10}$$

In Eq. (10), $P_{eq}(\Omega,\Xi)$ is the joint equilibrium probability distribution function in orientations Ω and Ξ. We shall invoke the assumption, based on the hypothesis that the collective motions associated with director fluctuations and those associated with single-particle reorientations have different characteristic time scales (i.e., a molecule reorients many times before the director fluctuates significantly), that $P_{eq}(\Omega,\Xi)$ can be factored into the equilibrium distributions $P_{eq,\Xi}(\Omega)$ and $f_{eq}(\Xi)$, so that[17]

$$P_{eq}(\Omega,\Xi) \cong P_{eq,\Xi}(\Omega)f_{eq}(\Xi). \tag{11}$$

Note that $P_{eq,\Xi}(\Omega)$ is the equilibrium distribution in Ω for arbitrary values of Ξ. [Equation (11) is analogous to a Born–Oppenheimer approximation in quantum mechanics.] When substituted into Eq. (10), this leads to

$$\langle \mathcal{D}^2_{MK}(\Omega) \rangle \cong \int d\Xi f_{eq}(\Xi) \int d\Omega\, P_{eq,\Xi}(\Omega) \mathcal{D}^2_{MK}(\Omega). \tag{12}$$

The spin relaxation in the motional-narrowing regime is determined by the correlation function for the Hamiltonian in Eq. (8). But since the entire time dependence in $\mathcal{H}_1(\Omega)$ is contained in $\mathcal{D}^2_{M,-K}(\Omega)$, it is sufficient to study the correlation functions for the latter, i.e.,

$$C_{M,-K,M',-K'}(t) \equiv \langle \mathcal{D}^2_{MK}(\Omega)\mathcal{D}^{2*}_{M'K'}(\Omega_0) \rangle$$
$$- \langle \mathcal{D}^2_{MK}(\Omega) \rangle \langle \mathcal{D}^{2*}_{M'K'}(\Omega_0) \rangle. \tag{13}$$

The calculation of these correlation functions is performed using Eq. (12), and leads to the result that $C_{M,-K,M',-K'}(t)$ in Eq. (13) can be written as the sum of three terms[17] as noted above: (i) $C^{(1)}_{M,-K,M',-K'}(t)$, which describes molecular reorientation under the potential $U(\Omega)$; (ii) $C^{(2)}_{M,-K,M',-K'}(t)$, which is due to relaxation that arises from fluctuations in Ξ (e.g., director fluctuations); and (iii) $C^{(3)}_{M,-K,M',-K'}(t)$, which represents a (negative) cross term between these two processes, but which bears a simple relation to (ii).[17]

The spectral density terms relevant to the present discussion arise from (ii) and (iii). If one includes order-pa-

rameter fluctuations in lowest order, it can be shown that only terms with $K=K'=0$ will enter the expression for $C^{(2)}_{M,-K,M',-K'}(t)$ and $C^{(3)}_{M,-K,M',-K'}(t)$. The analysis of the fluctuations in the order parameter leads to the result that the correlation function describing such fluctuations (when they are small) near the N–I transition are given by

$$C^{(2)}_{M,-K,M',-K'}(t)$$
$$= \tfrac{1}{25} \langle \bar\lambda(t=0)\mathcal{D}^{2*}_{M',0}(\Psi_0)\bar\lambda(t)\mathcal{D}^2_{M,0}(\Psi) \rangle \delta_{0,K}\delta_{0,K'}. \tag{14}$$

above the phase transition, and below the phase transition it is only necessary to replace $1/25$ by $\kappa(M,0)\kappa(M',0)$.[35] In Eq. (14), $\bar\lambda(t)$ is the (time-dependent) ordering potential, and Ψ denotes the instantaneous orientation of the local director in a lab-fixed frame (e.g., the mean director). In the case of a weakly ordered probe molecule with order parameter $S^{(p)}$ and ordering potential $\bar\lambda^{(p)}$, the approximate substitution $\bar\lambda^{(p)}/S^{(p)} \approx \bar\lambda/S$, which holds when $\bar\lambda$ is small, leads to

$$C^{(2)}_{M,-K,M',-K'}(t) \cong (S^{(p)}_{NI}/S_{NI})^2 \langle (Q^*_{M'})_0 (Q_M)_t \rangle \delta_{K,0}\delta_{K',0}. \tag{15}$$

The ratio $(S^{(p)}_{NI}/S_{NI})$ in Eq. (15) can be estimated from the measured order parameters for the probe and the liquid crystal just below the N–I transition. The fluctuations in $Q_M(q)$ (the nematic order tensor) appearing in Eq. (15) are described by Landau–de Gennes mean-field theory, leading to the result that the spectral densities for the order-parameter fluctuations are given by[17]

$$J^{(2)}_{M,-K,M',-K'}(\omega) \cong \left(\frac{S^{(p)}_{NI}}{S_{NI}}\right)^2 \frac{k_b T}{4\sqrt2 \pi}\left(\frac{\nu}{L^3\omega_\xi}\right)^{1/2}$$
$$\times \left\{\frac{1}{1+[1+(\omega/\omega_\xi)^2]^{1/2}}\right\}^{1/2}$$
$$\times \delta_{K,0}\delta_{K',0}\delta_{M,M'} \tag{16}$$

with

$$\omega_\xi = L/(\nu\xi^2). \tag{17}$$

In Eq. (16), L is a force constant for distortions, ν is the solvent viscosity, and ξ is a coherence length for order fluctuations. (Note that we have used k_b for Boltzmann's constant.) For small order fluctuations, ξ^2 is inversely proportional to $(T-T^*)$, since according to Landau–de Gennes theory, $\xi^2 = L/a(T-T^*)$. Equation (16), which applies above the N–I transition, may be used for below the transition by multiplying by $[5\kappa(0,M)]^2$ (cf. Appendix A) and letting $\nu \to \nu_N$, $L \to L_N$, and $\xi \to \bar\xi$.

The effects of finite translational diffusion can be incorporated into Eq. (16) by procedures described in detail in Appendix B in Ref. 17. One then has the result

$$J^{(2)}_{MK}(\omega) \approx \left(\frac{1}{4\pi}\right)\left(\frac{S^{(p)}_{NI}}{S_{NI}}\right)^2 \frac{k_b T\xi}{L}\delta_{K,0}$$
$$\times \left[\frac{D(1-(1/\sqrt2)\{[x^2+(\omega/\omega_\xi')^2]^{1/2}+x\}^{1/2}) + (\omega\xi^2/\sqrt2)\{[x^2+(\omega/\omega_\xi')^2]^{1/2}-x\}^{1/2}}{\omega^2\xi^4+D^2}\right] \tag{18}$$

with $\omega_\xi' \equiv L'/\nu\xi^2$, $L' \equiv L + \nu D$, and $x \equiv L/L'$. Note that the secular spectral densities are given by

$$J_{M0}^{(2)}(0) = \left(\frac{1}{4\pi}\right)\left(\frac{S_{NI}^{(p)}}{S_{NI}}\right)^2 \frac{k_b T\xi}{L}\left(\frac{1-\sqrt{x}}{D}\right)$$

$$= \left(\frac{1}{4\pi}\right)\left(\frac{S_{NI}^{(p)}}{S_{NI}}\right)^2 \frac{k_b T\xi}{LD}\left(1 - \frac{1}{\sqrt{1+\nu D/L}}\right). \tag{19}$$

Equations (16) and (18) show that $J^{(2)}(\omega)$ is largest at zero frequency; therefore, the secular spectral densities for order fluctuations are the dominant contributors to the anomalous part of spin relaxation. The anomalous contributions to the linewidth parameters B and C (cf. Sec. III), i.e., B_{anom} and C_{anom}, are given by (in G):[28,17]

$$B_{anom} = \frac{-\gamma_e B_0}{9}(A_{xx} + A_{yy}$$
$$- 2A_{zz})(2g_{zz} - g_{xx} - g_{yy})J_{00}(0) \tag{20}$$

and

$$C_{anom} = \frac{\gamma_e}{72}(A_{xx} + A_{yy} - 2A_{zz})^2[8J_{00}(0) - 3J_{10}(\omega_a)], \tag{21}$$

where the spectral densities in Eqs. (20) and (21) are given by Eq. (18); A_{ij} and g_{ij} are the Cartesian components of the hyperfine and g tensors, respectively; B_0 is the dc magnetic field; and ω_a is the frequency of nuclear spin flips. These substitutions lead to

$$B_{anom} = k_B(T - T^*)^{-1/2} \tag{22}$$

and

$$C_{anom} = k_C(T - T^*)^{-1/2}, \tag{23}$$

where k_B and k_C are given by (neglecting translational diffusion and the cross term $J_{MK}^{(3)}$):

$$k_B = \left[-\frac{\gamma_e B_0}{9}(A_{xx} + A_{yy} - 2A_{zz})\right.$$
$$\left.\times(2g_{zz} - g_{xx} - g_{yy})\left(\frac{S_{NI}^{(p)}}{S_{NI}}\right)^2\right]\left(\frac{k_b T\nu}{8\pi L^{3/2}a^{1/2}}\right) \tag{24}$$

and

$$k_C = \left[\frac{\gamma_e}{72}(A_{xx} + A_{yy} - 2A_{zz})^2(N_C)\left(\frac{S_{NI}^{(p)}}{S_{NI}}\right)^2\right]$$
$$\times\left(\frac{k_b T\nu}{8\pi L^{3/2}a^{1/2}}\right). \tag{25}$$

In Eq. (25), N_C is a factor which takes on values between 8 and 5;[36] the former limit corresponds to the case when $J_{10}(\omega_a) \ll J_{00}(0)$ (which is the case for slow fluctuations and/or molecular diffusion), whereas the latter limit corresponds to $J_{10}(\omega_a) \approx J_{00}(0)$ (which occurs in the case of rapid fluctuations). The quantities appearing within the first set of braces in these equations for k_B and k_C depend solely upon the properties of the spin probe, while the second set contains parameters characteristic of the liquid crystal. In order to provide order-of-magnitude estimates, we use the

parameters for N-(P-methoxybenzylidene)-p-n-butylaniline (MBBA), i.e., $L \approx 10^{-6}$ dyn, $a \approx 6 \times 10^5$ ergs/cm³ °C, $\nu = 0.3$ P.[37,16] We estimate the quantity within the second set of square brackets in Eqs. (24) and (25) to be ca. 1.05×10^{-9} at $T_{NI} \approx 78$ °C, which is the N–I transition temperature for 4O,6 (T_{NI} for 6OCB–8OCB is 79 °C at the composition studied). k_B and k_C can thus be estimated from a knowledge of the probe ordering and the magnetic tensors. Note, however, that when the more general expression, i.e., Eq. (19), is used, one finds that the secular spectral densities including translational diffusion are $2x/(1 + \sqrt{x})$ times those calculated neglecting the effects of D.

We note that C_{anom}/B_{anom} lies between the limits $(8/5)(C_0/B_0)$ and (C_0/B_0) depending on the value of N_C. Equations (20) and (21) also show that for isotropic diffusion in isotropic liquids (or in ordered phases when the ordering of the spin probe is low) the temperature dependence of B_{anom} and C_{anom} can alternatively be described by the equations

$$\frac{B_{anom}}{5B_0} = \frac{C_{anom}}{N_C C_0} = k'(T - T^*)^{-1/2}, \tag{26}$$

where

$$k' = \left(\frac{S^{(p)}}{S}\right)^2 \frac{k_b T}{4\pi L^{1/2}a^{1/2}D}\left(1 - \frac{1}{\sqrt{1+\nu D/L}}\right)\tau_R^{-1}. \tag{27}$$

k can be calculated from the order parameters $S^{(p)}$ and S (i.e., for the probe and liquid crystal solvent, respectively) at the N–I transition, the physical properties of the liquid crystal, and the rotational correlation times of the spin probe near T_{NI}. The modifications required when the probe orders with an asymmetric potential are described in Appendix A. They are the forms utilized to analyze the experiments on PD-tempone.

B. N–S_A transition

While the weakly first-order transition is satisfactorily understood in terms of mean-field theory, this is not the case for the N–S_A transition which is often second order[38] and to which dynamic scaling laws analogous to the λ transition in He have been applied.[19,39] Models based on dynamic scaling show that as the N–S_A transition is approached, the elastic constants for twist and bend deformations K_2 and K_3 diverge as $(T - T^*)^{-2/3}$.[39,40] This implies that the spectral density contribution due to order-director fluctuations, which are proportional to $K^{-3/2}$ (Ref. 17) (where K is the average elastic constant of the liquid crystal), must be *suppressed* as the transition is approached. That is, as T^* is approached from the nematic phase, the linewidth parameters [see Eq. (1)] would be affected as follows: A would decrease, B would be unaffected, and C would increase. However, the experimental fact that all three parameters are noted to increase (see Sec. V) demonstrates that director fluctuations and their suppression near the phase transition do not play a major role in influencing relaxation near the N–S_A transition.

The model we use for interpreting our relaxation results at the N–S_A transition was proposed by Zager and Freed,[20] and is presented in detail in paper I. As T^* is approached from the nematic phase, smectic layers begin to form as a pretransitional effect. The formation of such layers (cybotactic clusters) is described by fluctuations in the smectic order parameter, which leads to density fluctuations $\rho(\mathbf{r},t)$. During the formation of cybotactic clusters, the movement of probe molecules from the aromatic core regions in the liquid crystals to the (lower density) chain regions[22,27] affects the order parameter S and/or rotational correlation time τ_R of the probe. Thus density fluctuations which cause the cybotactic clusters to form and break up in different spatial regions, modulate the molecular dynamics and therefore the spin relaxation of the probe directly.

The description of fluctuations in the smectic order parameter requires the use of two correlation lengths $\xi_\perp$ and $\xi_\parallel$ which diverge with different power-law exponents $\nu_\perp$ and $\nu_\parallel$, i.e., as $(T - T_c)^{-\nu_\perp}$ and $(T - T_c)^{-\nu_\parallel}$, respectively. In the Landau description one has critical exponents $\nu_\perp = \nu_\parallel = 1/2$. From the superfluid analogy, one still expects $\nu_\perp = \nu_\parallel$, but with a higher numerical value, i.e., 2/3. Experimentally, however, these exponents are noted to vary between 0.9 and 0.5; an observation which, as yet, has only partially been explained by the renormalization-group calculations which predict a crossover in critical exponents near the tricritical point.[10,41,42]

The relaxation of the S_A order parameter $\Psi(\mathbf{r},t)$ is described by the following rate law for the qth mode of fluctuation [cf. Eqs. (9)–(11) of paper I as well as Ref. 21 of paper I]:

$$\langle \Psi^*(\mathbf{q},t)\cdot\Psi(\mathbf{q},0)\rangle = \langle |\Psi(\mathbf{q})|^2\rangle \exp(-t/\tau_q), \qquad (28)$$

where $\Psi(\mathbf{q},t)$ is the Fourier transform of $\Psi(\mathbf{r},t)$, and above the N–S_A transition it denotes the mean-square displacement in the order parameter:

$$\langle |\Psi(\mathbf{q})|^2\rangle \equiv \alpha_q^{-1} = \frac{k_b T}{2AV}\frac{1}{(1 + q_\perp^2 \xi_\perp^2 + q_\parallel^2 \xi_\parallel^2)}, \qquad (29)$$

and τ_q is the q-dependent relaxation time of the smectic order parameter given by

$$\tau_q = \frac{\tau_m}{(1 + q_\parallel^2 \xi_\parallel^2 + q_\perp^2 \xi_\perp^2)^x}, \qquad (30)$$

which is a simple interpolation form that satisfies dynamic scaling as discussed below. In these equations, $\xi_\perp$ and $\xi_\parallel$ are the coherence lengths parallel and perpendicular to the mean director (the z axis), respectively, and $q_\parallel$ and $q_\perp$ are the respective components of $\mathbf{q}$. Also, V is the sample volume, and A is the coefficient in the term quadratic in the Landau expansion of the smectic free energy (see Appendix B). τ_m is a relaxation time that is independent of $\mathbf{q}$ and is expected to vary as $|T - T_{NA}|^{-1}$.[39] The exponent x is determined from dynamic scaling arguments. The argument due to Brochard goes as follows. τ_q is considered to be a homogeneous function of τ_m and $(\mathbf{q}\cdot\xi)$, i.e., $\tau_q = \xi^z f(q\xi)$ (assuming isotropic correlation lengths) with $f(q\xi) \propto (q\xi)^{-z}$ at

large $q\xi$, which defines the dynamic scaling for isotropic systems. At $T = T_{NA}$, τ_m diverges as ξ^z, i.e., the $q = 0$ mode becomes infinitely slow; this is the so-called critical slowing down of the order parameter. For larger values of q, however, τ_q does not diverge as $T \to T_{NA}$. From Brochard's argument,

$$\tau_q = \bar{f}(\tau_m, \mathbf{q}\cdot\xi) \equiv \tau_m f(q\xi) \propto [1/(T - T_{NA})]f(q\xi), \qquad (31)$$

i.e., $\tau_m \propto \xi^z$ with $z = 3/2$; and therefore, in order to have a nondivergent τ_q for $q\xi \to \infty$ near the NA transition, we estimate x as follows [cf. Eqs. (30) and (31)]:

$$\tau_q \approx \tau_m/(q\xi)^{2x} \propto |T - T_{NA}|^{-1 + 2x\nu}/q^{2x} \quad \text{as } q \to \infty. \quad (31a)$$

Hence, we must have $2x\nu = 1$. If $\nu = 2/3$ (from the superfluid analogy) one has $x = 3/4$; or if $\nu = 1/2$ (Landau theory) then $x = 1$. Dynamic scaling, as well as its anisotropy for the N–S_A transition, is further discussed in Appendixes B and C. Having determined both the amplitude as well as the decay rates of Ψ, we now proceed to consider how the fluctuations in Ψ affect the relevant molecular spectral densities associated with $\mathscr{H}_1(\Xi)$.

The formalism for the treatment of the correlation functions for spin relaxation at the N–S_A transition has been discussed elsewhere[20,21] but is briefly summarized here. The time-dependent fluctuations in the relaxation parameter(s) Q (where Q could, for example, be S or τ_R) are proportional to fluctuations in the density:

$$\langle \Delta Q(r_B,t)\Delta Q(r_B,0)\rangle \propto \langle \Delta\rho(r_B,t)\Delta\rho(r_B,0)\rangle, \qquad (32)$$

where (r_B,t) refers to the position of the Brownian particle at time t, and $\Delta\rho \equiv (\rho - \rho_0)$ denotes the deviation of the density ρ from its mean value ρ_0. The translational diffusion of the probe is taken to obey a Smoluchowski equation with a time-dependent potential of mean force (acting on the probe), which is a functional of the density fluctuations (i.e., $U(r,t) = U[\Delta\rho(r,t)]$). Then $\Delta\rho(r,t)$ is related to the complex smectic order parameter $\Psi(r,t)$ in the usual manner.[39]

In the spirit of a Landau expansion, only the lowest order terms in $\Delta\rho(\mathbf{r})$ are considered in the time-dependent fluctuations in spin-relaxation parameters. The method of approach for calculating the relevant correlation functions and spectral densities including the critical hydrodynamics of the phase transition and the translational diffusion of the probe is based upon methods previously developed[17] and is discussed in paper I (Ref. 21). One obtains the result [cf. Eqs. (28)–(30) of paper I]

$$J(\omega) = \text{Re}\int_0^\infty C(t)e^{-i\omega t}dt, \qquad (33)$$

where

$$C(t) = \frac{V}{4(2\pi)^3}\int_0^{q_c} d^3q\, \alpha_{q-q_s}^{-1}$$

$$\times \exp[(-\tau_{q-q_s}^{-1} + D_\parallel q_\parallel^2 + D_\perp q_\perp^2)t]. \qquad (34)$$

In Eq. (34), τ_{q-q_s} and $\alpha_{q-q_s}^{-1}$ are as defined by Eqs. (30) and (29), respectively, but with $q_\parallel$ replaced by $(q_\parallel - q_s)$, where q_s is the wave vector corresponding to the interlayer spacing in the S_A phase (i.e., $q_s = 2\pi/d$, where d is the thickness of a

smectic layer), and it lies along the director (thus along $q_\parallel$). The solutions of Eqs. (33) and (34) require, in general, numerical computations. One can, however, obtain some physical insight by considering special limiting cases which admit of analytical solutions.[21]

Let us first ignore anisotropies by setting $\xi_\parallel = \xi_\perp$, $D_\parallel = D_\perp$, and take the dynamic critical exponent as $x = 1$. We obtain a simple analytic form in the limits that $D_\parallel q_s^2 \tau_m \to 0$ (by simply letting $q_s \to 0$) and $q_c \to \infty$. This ignores the effect of diffusion of the probe *through* the smectic layer. One obtains for $J(\omega)$[43]

$$4J(\omega) = \frac{Mk_b T}{4\pi} \xi \left(D \left\{ 1 - \left(\frac{1}{2} z \right)^{1/2} \right. \right.$$

$$\left. \times \left[(1 + \omega^2 \tau_m^2)^{1/2} + 1 \right]^{1/2} \right\}$$

$$\left. + \frac{1}{\sqrt{2}} \omega \xi^2 z^{1/2} \left\{ \left[1 + \omega^2 \tau_m^2 \right)^{1/2} - 1 \right]^{1/2} \right\} \right)$$

$$\times \frac{1}{\omega^2 \xi^4 + D^2}, \qquad (35)$$

where $M \equiv (2A\xi^2)^{-1}$, and $z \equiv (1 + D\tau_m / \xi^2)^{-1}$ measures the relative importance of translational diffusion over the correlation length ξ, vs relaxation of the smectic ordering in providing averaging of the fluctuations in Q. For $z \ll 1$ the former dominates, whereas for $z \approx 1$ the latter dominates. The spectral density at zero frequency makes the dominant contribution to the ESR linewidth near the critical region, and from Eq. (35) it is

$$4J(0) = \frac{Mk_b T}{4\pi} \frac{z\tau_m}{\xi(1 + z^{1/2})}$$

$$\xrightarrow{z \approx 1} \frac{Mk_b T}{8\pi} \frac{\tau_m}{\xi} \propto \xi^{1/2} \propto (T - T_{NA})^{-1/3}$$

$$\xrightarrow{z \ll 1} \frac{Mk_b T\xi}{8\pi D} \propto \xi \propto (T - T_{NA})^{-2/3}. \qquad (36)$$

Based upon measurements of $\xi_\parallel$ (Refs. 10 and 42) and D (Refs. 44, 45, and 46) in somewhat related materials, and estimates of τ_m (Ref. 20) (cf. Tables IV and V), $D_\parallel \tau_m / \xi^2 \approx 10^{-2}$ to 10^{-3} (for $T - T_c \approx 0.1$ °C), while $D_\parallel \tau_m q_s^2 \approx 10^3$ to 10^2. Thus, while it may be reasonable to ignore the averaging effects of translational diffusion over the distances of $\xi_\parallel$, it would appear questionable to let $D_\parallel \tau_m q_s^2 \to 0$, i.e., ignoring diffusional averaging over a single smectic layer of thickness d. However, it is pointed out in paper I and by Zager and Freed that Eq. (35) is the appropriate solution to the model wherein the probe is expelled to the alkyl regions upon forming smectic clusters; i.e., there is a nonequilibrium distribution of probe relative to position in a smectic layer, and the probes rapidly adjust their position relative to the liquid-crystal molecules as the smectic clusters form and break up. Thus, even with a substantial diffusion coefficient $D_\parallel$, it would not average out the effect. This point of view is supported by recent ESR studies within the smectic phase which were interpreted in terms of a nonuniform probability distribution for different heights within the bilayer.[50]

We can also consider Eq. (34) in the case where $q_s = 2\pi/d$ is finite and let $D_\parallel \tau_m / \xi_\parallel^2$, $D_\perp \tau_m / \xi_\perp^2$ approach

TABLE IV. Linear least-squares analysis of fits to theoretical spectral density for the N–S_A transition of 4O,7: $\ln J(0) = \ln k + \sigma \ln(T - T_c)$, where $J(0)$ is given by Eq. (88).[a,b]

No.	$D_\perp$	$D_\parallel$	τ_m^0	q_s	σ^c	$\ln(k)^c$	rms dev.
1	0	0	1.6	0	-0.360	-17.135	8.59×10^{-3}
2					(-0.370)	(-17.813)	1.16×10^{-2}
3	2	2	1.6	0	-0.480	-18.245	1.44×10^{-2}
4					(-0.426)	(-18.222)	1.56×10^{-2}
5	0	0	1.6	0.234	-0.359	-17.354	8.22×10^{-3}
6					(-0.367)	(-18.494)	1.08×10^{-2}
7	2	2	1.6	0.234	-0.048	-20.763	6.85×10^{-3}
8					(-0.007)	(-20.891)	3.98×10^{-3}
9	5.9	4.7	1.6	0	-0.542	-18.699	1.44×10^{-2}
10					(-0.471)	(-18.614)	1.73×10^{-2}
11	5.9	4.7	0.16	0	-0.448	-19.729	1.40×10^{-2}
12					(-0.391)	(-20.259)	1.28×10^{-2}

[a] Units of the quantities shown in the table are as follows: $D_\perp$, $D_\parallel$ in 10^{-7} cm²/s; τ_m^0 in 10^{-8} s; q_s in 10^8 cm^{-1}.

[b] Parameters not shown in the table are as follows (however, see footnote c below): $M_v = (2A\xi_\parallel^2)^{-1} = 5.38 \times 10^5$ cm/ergs; $T_c = 55$ °C; $\xi_\perp^0 = 1.07$ Å, $\xi_\parallel^0 = 6.63$ Å; $\nu_\perp = 0.65$, $\nu_\parallel = 0.78$; $\gamma = 1.46$; $\zeta = -0.94$; $x_\perp = 0.72$, $x_\parallel = 0.60$ Å; $q_{\perp,c} = 0.2337$ Å^{-1}, $q_{\parallel,c} = 1.4022$ Å^{-1}.

[c] The values of σ and $\ln(k)$ shown in parentheses were calculated using the same parameters as in the preceding case with the following exceptions: $\xi_\perp^0 = \xi_\parallel^0 = 2.9$ Å; $\nu_\perp = \nu_\parallel = 2/3$; $\gamma = 4/3$; $\zeta = -1.0$; $x_\perp = x_\parallel = 3/4$; $q_{\perp,c} = q_{\parallel,c} = 0.2337$ Å^{-1}.

TABLE V. Linear least-squares analysis of fits to theoretical spectral density for the N–S_A transition of 6OCB–8OCB: $\ln J(0) = \ln k + \sigma \ln(T - T^*)$, where $J(0)$ is given by Eq. (88).[a,b]

No.	$D_\perp$	$D_\parallel$	τ_m^0	q_s	σ^c	$\ln(k)^c$	rms dev.
1	0	0	2.0	0	-0.425	-18.591	3.38×10^{-3}
2					(-0.348)	(-19.633)	6.73×10^{-3}
3	2	2	2.0	0	-0.453	-18.807	6.14×10^{-3}
4					(-0.354)	(-19.671)	7.58×10^{-3}
5	0	0	2.0	0.206	-0.424	-19.279	2.94×10^{-3}
6					(-0.347)	(-20.320)	6.43×10^{-3}
7	2	2	2.0	0.206	-0.116	-21.302	3.19×10^{-3}
8					(-0.002)	(-22.135)	2.37×10^{-3}
9	5.9	4.7	2.0	0	-0.481	-19.048	8.05×10^{-3}
10					(-0.364)	(-19.733)	7.07×10^{-3}
11	5.9	4.7	0.20	0	-0.435	-20.972	4.49×10^{-3}
12					(-0.350)	(-21.946)	6.97×10^{-3}

[a] Units of the quantities shown in the table are as follows: $D_\perp, D_\parallel$ in 10^{-7} cm²/s; τ_m^0 in 10^{-8} s; q_s in 10^8 cm^{-1}.

[b] Parameters not shown in the table are as follows (however, see footnote c below): $M_v = (2A\xi_\parallel^2)^{-1} = 4.94 \times 10^5$ cm/ergs; $T_c = 45$ °C; $\xi_\perp^0 = 7.3$ Å, $\xi_\parallel^0 = 24.0$ Å; $\nu_\perp = 0.60$, $\nu_\parallel = 0.78$; $\gamma = 1.48$; $\zeta = -0.91$; $x_\perp = 0.76$, $x_\parallel = 0.58$; $q_{\perp,c} = 0.206$ Å^{-1}, $q_{\parallel,c} = 1.236$ Å^{-1}.

[c] The values of σ and $\ln(k)$ shown in parentheses were calculated using the same parameters as in the preceding case with the following exceptions: $\xi_\perp^0 = \xi_\parallel^0 = 12.9$ Å; $\nu_\perp = \nu_\parallel = 2/3$; $\gamma = 4/3$; $\zeta = -1.0$; $x_\perp = x_\parallel = 3/4$; $q_{\perp,c} = q_{\parallel,c} = 0.206$ Å^{-1}.

zero (which they do as $\xi^{-1/2}$). Then, we obtain for the zero-frequency spectral density[20]

$$J(0)^{\text{crit}} \approx \frac{M k_b T}{16\pi} \frac{\tau_m}{\xi} \frac{\sqrt{1+c}-1}{c}. \qquad (37)$$

In Eq. (37), $c = q_s^2 D_\parallel \tau_m$. It measures the relative importance of averaging out the effects of density fluctuations $\Delta\rho(\mathbf{r})$ in a single smecticlike layer through diffusion of the probe in the direction normal to the layer vs the relaxation of the smectic layers. As $c \to 0$, corresponding to probe diffusion being unimportant, one has $J(0) \propto \tau_m/\xi \propto \xi^{1/2} \propto |(T - T_c)|^{-1/3}$. This is equivalent to the result of Eq. (36) in the limit $z \to 1$. For $c \gg 1$, $J(0) \propto \tau_m^{1/2}/\xi \propto \xi^{-1/4}$, and it does not diverge, but rather goes to zero. This model does not include the expulsion effect referred to in the previous paragraph.

For actual comparisons with experimental results we found it necessary to obtain numerical solutions to Eqs. (33) and (34). In those solutions, we could take account of the asymmetric critical exponents for $\xi_\parallel$ and $\xi_\perp$ as well as asymmetric dynamic scaling discussed in Appendix B. These numerical solutions are summarized in Appendix C, and they illustrate how the critical exponents for $J(0)$ are sensitive functions of these parameters as well as of $D_\parallel$ and $D_\perp$, although key qualitative features summarized by Eqs. (36) and (37) persist.

V. RESULTS AND DISCUSSION

The variation of B and C with temperature is shown in Figs. 3(a)–3(c) and 3(d)–3(e) for the various probes in 4O,6 and 6OCB–8OCB, respectively. Here, one clearly

notes that as the phase transitions are approached, the relaxation parameters exhibit anomalous behavior in that they appear to diverge. A closer look at these effects is presented in Figs. 4–6, where we show B and C for the transitions occurring in PD-tempone in 6OCB–8OCB as an example, along with the error bars associated with the linewidth measurements. The curves shown through the data points represent nonlinear least-squares fits using Eq. (2), as discussed in Sec. III. The results, shown in Tables II and III, together with the standard deviations, are discussed first for the N–I transition.

A. N–I transition

The results of the analysis at the N–I transition (cf. Table II) indicate that (i) in *all* cases, $\sigma = -1/2$; (ii) at a given transition, the value of T^* is higher at the lower-temperature phase than that obtained from the analysis at the higher-temperature phase; and (iii) for a given liquid-crystal solvent, the values of k, and their ratios obtained from the B and C analyses, depend on the spin probe. The exponent of $-1/2$ is rationalized in terms of the fact that it is the secular spectral density that contributes most to relaxation, and for nematic order fluctuations, it diverges as ξ. The observed divergence in the linewidth parameters is explained by invoking the result that for the coherence length of the order fluctuations, $\xi^2 \sim |T - T^*|^{-1}$. The observation that T^* appears to be higher for the analysis from the nematic than the isotropic side is consistent with previous studies of critical effects at the N–I transition seen with PD-tempone in MBBA.[16] For T_c as the actual N–I phase-transition temperature, Rao, Hwang, and Freed[16] showed that if $T^\dagger$ and T^* denote the transition temperatures when the analysis at the N–I transition is performed from the N and I phases, respectively, then $T^\dagger \cong T_c + (T_c - T^*)/2$. Thus, when $T_c - T^* \approx 1$ °C, we expect $T^\dagger \cong T_c + 0.5$, which is on the order of the observed difference.

The relative contributions of the critical effects to spin relaxation are, as noted in Eq. (26), measured by the parameters k_B and k_C. Though the *absolute* values of k_B and k_C depend on the properties of the liquid crystal, the ratio $B_{\text{anom}}/C_{\text{anom}}$ (or equivalently k_B/k_C) is independent of the properties of the solvent (except for the small dependence on the solvent of the magnetic tensors for a given probe) as well as the extent of probe ordering [see Eqs. (24) and (25)], and it depends only on the ratio of the anisotropy of the g and A tensors and the parameter N_C, i.e.,

$$\frac{B_{\text{anom}}}{C_{\text{anom}}} = \frac{k_B}{k_C} = \frac{8B_0 [g_{zz} - (g_{xx} + g_{yy})/2]}{N_C [A_{zz} - (A_{xx} + A_{yy})/2]}. \qquad (38)$$

This ratio therefore provides a useful means of assessing the experimental results in cases where the relevant liquid-crystal data are unavailable. In the isotropic phase, one expects this ratio to remain constant with temperature for motions for which $\omega_a^2 \tau_C^2 \ll 1$ (i.e., when secular and pseudosecular spectral densities make equal contributions to relaxation), and for which $N_C = 5$. This is typically the case with PD-tempone. On the other hand, when $\omega_a^2 \tau_C^2 \gg 1$, the pseudosecular terms are smaller, and $N_C = 8$.
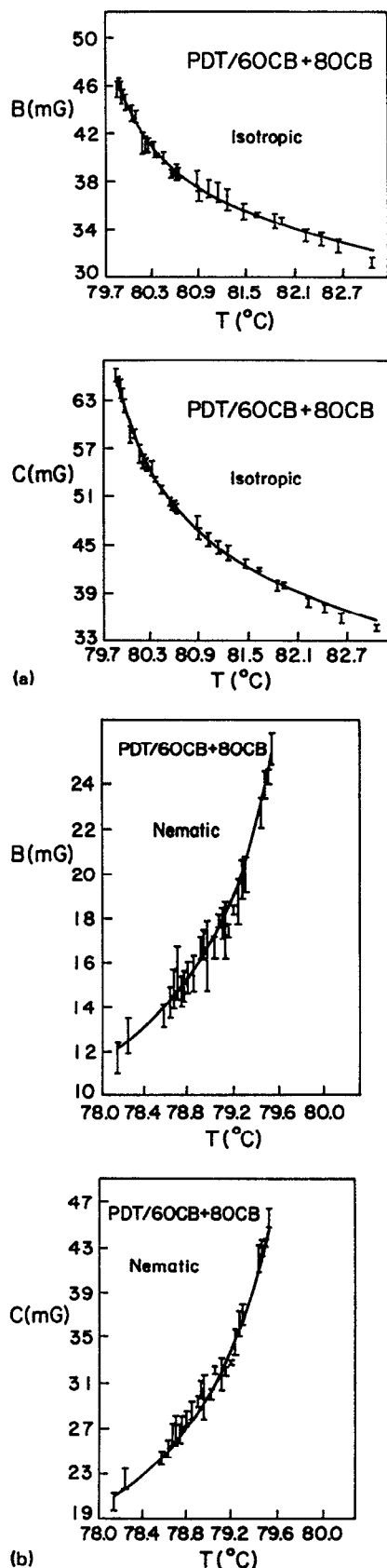
FIG. 4. Temperature variation of linewidth parameters B and C for PD–tempone in 6OCB–8OCB at (a) I–N transition, and (b) N–I transition. The curve through the data points represents the fit based on the critical terms (see text). The parameters used for the fits are tabulated in Table II.
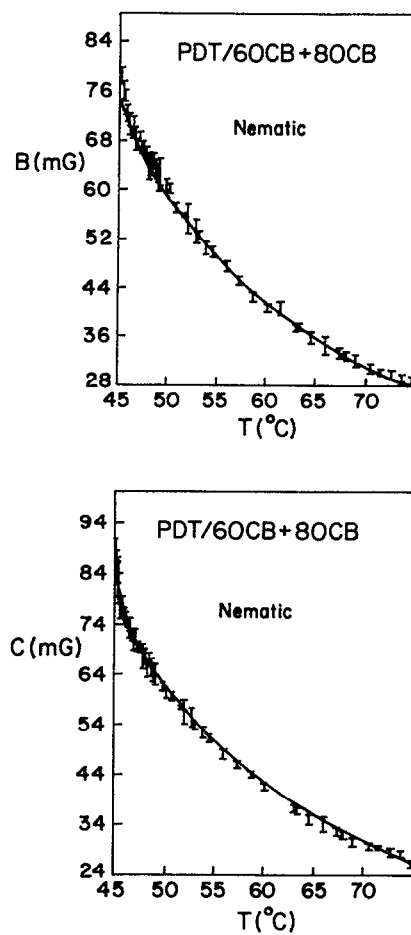

FIG. 5. Temperature variation of linewidth parameters B and C for PD–tempone in 6OCB–8OCB at N–S_A transition. Parameters used in the fits are shown in Table III.

Using the magnetic tensors for the three spin probes in Table I, the order parameters for spin probes in 6OCB–8OCB and 4O,6 (Refs. 22, 27, and 47) relative to the liquid-crystal ordering [as measured using CSL (defined in Fig. 1), $S \approx 0.4$], and the parameters for MBBA in Eqs. (26) and (27), the values of k_B and k_C were estimated for the cases corresponding to x and y ordering, i.e., for those cases for which the x or y axis of the magnetic tensor frame lies along the ordering axis (usually assumed to be coincident with the principal axis of diffusion) of the spin probe. The results of such calculations are now summarized.

1. PD–Tempone in 6OCB–8OCB

As the N–I transition is approached from above (I phase), $C_{\text{anom}}/B_{\text{anom}}$ changes from near unity to about 1.5. This implies that away from the transition, the pseudosecular and secular terms are comparable, but near T_{NI} the pseudosecular spectral densities become smaller compared to the secular spectral densities [cf. Eqs. (20) and (21)]. The ratio of these two terms is given by [see Eq. (16)].

$$\frac{J(0)}{J(\omega_a)} = \frac{\{1 + [1 + (\omega_a/\omega_\xi)^2]^{1/2}\}^{1/2}}{\sqrt{2}}.$$
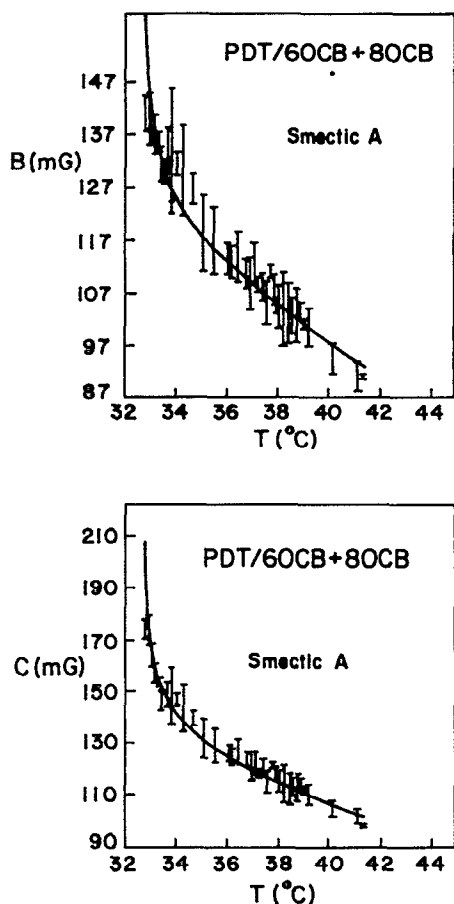
FIG. 6. Temperature variation of linewidth parameters B and C for PD–tempone in 6OCB–8OCB at S_A–RN transition. Parameters used in the fits are shown in Table III.

Using parameters for MBBA, we estimate $J(0)/J(\omega_a) = 2.8$ at $(T - T^*) = 1$ °C. As the transition is approached, this ratio increases, causing C_{anom}/B_{anom} to approach 1.6, thus reasonably consistent with the observed result. In the analysis discussed in the next paragraph we therefore used $N_C = 8$.

Previous studies of spin relaxation using PD-tempone in liquid-crystal solvents have shown that PD-tempone aligns with its magnetic y axis along the principal ordering axis, a phenomenon referred to as "y ordering",[27,22] and furthermore, that its ordering exhibits a significant nonaxially symmetric component. The relaxation expressions for order-parameter fluctuations developed earlier (see above, and Ref. 17), which assumed a cylindrically symmetric ordering potential, are, in fact, found to be inadequate (cf. below). More general expressions than Eqs. (24) and (25) for k_B and k_C, which take into account the anisotropic nature of the ordering, are developed in Appendix A, and the results are used here. Using solvent parameters for MBBA [i.e., ν and L; cf. discussion below Eq. (25)], $S^{(p)}/S \approx 0.25$, and using y ordering for PD-tempone in 6OCB–8OCB, we calculate [using Eqs. (A26) and (A27) in Appendix A, with $\lambda = 0.42$ and $\rho = 0.042$] $k_B = 31$ mG, and $k_C = 73$ mG, and therefore $k_C/k_B = 2.35$. The calculated values of k_B and k_C can-

not be directly compared with the experimental values (14.2 and 46.4 mG, respectively), because the solvent parameters for MBBA have been used, since those for 6OCB–8OCB are not known. Nevertheless, given that uncertainty, they appear to agree well within factors of 2. The solvent-independent ratio, k_C/k_B is 3.3 ± 0.6, and is in reasonable agreement with the theoretical value of 2.4. The importance of using the full asymmetric formulas is illustrated by treating PD-tempone as a probe whose ordering potential is cylindrically symmetric; then k_C/k_B is calculated to be *abnormally* high (21.7).

The values of k_B and k_C at the nematic side of the transition are similarly calculated using Eqs. (A28) and (A29) in Appendix A. For 6OCB–8OCB, we obtain $k_B = 16.9$ and $k_C = 39.8$, and hence $k_C/k_B = 2.36$. Experimentally, k_C/k_B is about 1.84, which is in fairly good agreement with the calculated value. However, whereas the values of k_B and k_C are predicted to decrease by a factor of 1.8 from those of the isotropic side, in reality they are observed to remain at roughly the same the same level. (More precisely, B is observed to remain constant, whereas C does decrease by a factor of 1.55.)

2. MOTA in 6OCB–8OCB

MOTA in 6OCB–8OCB shows very low ordering, and one therefore expects that the critical contributions to relaxation (which are proportional to the square of the order parameter) will be small. Indeed, no critical divergence is observed at the N side of the N–I transition. On the I side, however, a five-parameter fit gave a critical exponent of $-1/2$; but when the F test (see above) was used to compare the results of a five-parameter vs a (nested) two-parameter fit representing the Arrhenius term alone, the value of $P_F(\nu_1, \nu_2; F)$ was 86%, which is not convincing evidence in favor of the five-parameter fit. A probable reason for a small critical contribution to relaxation is that MOTA resides mainly among the chain regions in this solvent yielding the low ordering, and is thus insensitive to the order fluctuations that drive the N–I transition.

The values of k_B and k_C were calculated in the isotropic phase using the magnetic tensors in Table I, and, as before, the parameters for MBBA. The order parameter just below the N–I transition was 0.048.[22] From Eqs. (24) and (25), we calculate (using $N_C = 8$ for k_C) $k_B = 29.1$ and $k_C = 23.1$, or $k_C/k_B = 0.79$ (note that x ordering was assumed for MOTA). The absolute values of k_B and k_C thus calculated agree within a factor of 1.7 of the experimental values ($k_B = 42.0$ and $k_C = 39.0$), and k_C/k_B lies well within the experimental uncertainty associated with the absolute values of k_B and k_C that were measured (0.98 ± 0.48).

3. PD–Tempone, MOTA, and P in 4O,6

The order parameters for the three probes in 4O,6 increase in the order PD-tempone < MOTA < P, and at the N–I transition are roughly 0.03, 0.07, and 0.15.[27,22,47] Thus, k_B and k_C increase in this order. This is predicted theoretically and observed experimentally (cf. Table II).

Once again k_C/k_B calculated for PD-tempone using the assumption of cylindrical symmetry for the ordering potential (0.73) is much lower than the experimental value of 2.29. As before, using the anisotropic ordering potential (Appendix A), y ordering [with $\lambda = 0.23$ and $\rho = 0.085$ (Ref. 27)], and $S^{(p)}/S \approx 0.1$ for 4O,6, we find that, at the isotropic side, $k_B = 4.25$, $k_C = 10.21$, and that $k_C/k_B = 2.40$, which is very good agreement with experiment. (The experimental k's, 7.6 and 17.4, lie within a factor of 2 of the calculated values based on the parameters for MBBA). At the nematic side of the N–I transition, we calculate $k_B = 2.1$ and $k_C = 5.04$, or $k_C/k_B = 2.40$, which compares well with the observed value of 2.17, but again the predicted absolute values of k_B and k_C are about a factor of 2 smaller than those observed.

In the case of MOTA we predict on the isotropic side, $k_B = 40.8$, $k_C = 28.1$, or $k_C/k_B = 0.689$, whereas experimentally we observe $k_B = 58.4$ and $k_C = 68.3$ or $k_C/k_B = 1.17$. On the nematic side, we predict $k_B = 27.1$, $k_C = 18.6$ or $k_C/k_B = 0.686$, and this compares with the experimental values of $k_B = 43$, $k_C = 44$ or $k_C/k_B = 1.02$. In the case of P-probe, we predict on the isotropic side $k_B = 56.9$, $k_C = 41.0$, or $k_C/k_B = 0.72$ vs the experimental results of $k_B = 161$, $k_C = 76.6$, or $k_C/k_B = 0.475$. For the nematic side we predict $k_B = 37.8$, $k_C = 27.3$, or $k_C/k_B = 0.723$ vs the observed values of $k_B = 210$, $k_C = 125$, or $k_C/k_B = 0.595$. In the cases of MOTA and P-probe we have not corrected our predictions for any asymmetry in the ordering tensor, because the asymmetry was found to be small in the nematic phase. However, corrections for any small asymmetry might lead to improvement in the comparison between the k_B/k_C predicted and that actually observed. Another question is the precise value of S_p to use in the nematic phase. We used the value of 0.053 for MOTA and 0.070 for P-probe measured < 1 °C below the transition. However, just a few degrees below the transition, one observes S_p increases to 0.015 for MOTA and 0.260 for P-probe, whereas the value for CSL monitoring S_s does not change as much with temperature.

4. General comments

The values of k_B and k_C at the nematic side of T_{NI} are obtained by replacing ξ $[\xi^2 \approx L/a(T - T^*)]$ by $\bar{\xi}$ $[\bar{\xi}^2 \approx L/3a(T^* - T)]$ in Eq. (18). Since the spectral densities are proportional to ξ [cf. Eq. (18)] this substitution implies a reduction in the k values in the nematic phase by a factor of $\sqrt{3}$.[16] The other factors that can cause changes in k during phase transformation are τ_R and D [cf. Eq. (27)]. However, τ_R does not change very much upon passing from I to N,[27] and for $10^{-7} < D < 10^{-6}$ cm^2/s and typical values of v (0.3 P) and L (10^{-6} dyn), $vD/L \approx 0.03$ to 0.30 and one finds from Eq. (27) that

$$k' \approx (S^p/S)^2 \cdot k_b Tv/8\pi L^{3/2} a^{1/2} \tau_R^{-1},$$

i.e., k' is independent of D to a good approximation. Although we note that for PD-tempone in 4O,6, k' in the nematic phase is lower than in the isotropic phase, the values of k' seem to be comparable in the two phases in the other sys-

tems,[16] and for P in 4O,6, they are actually *higher* in the N phase. It is possible that at the weakly first order N–I transition, the changes in $v/L^{3/2}$ [cf. Eqs. (22) and (23)] with temperature may occur in a way such as to offset the decrease in k' by the factor of $\sqrt{3}$. In fact, it may be reasonable to suppose that v becomes greater in the nematic phase. However, we suspect that the use of a simple factor $(S^{(p)}/S)^2$ [as well as the factor $\kappa(K,M)$ calculated for the nematic side] do not adequately represent the manner in which the probe molecules couple to the order fluctuations. If the probe molecules preferentially relocate relative to the liquid-crystal molecules (e.g., to be preferentially located near the cores rather than the chain regions) on the nematic side of the transition, then one would expect trends more consistent with what is observed experimentally.
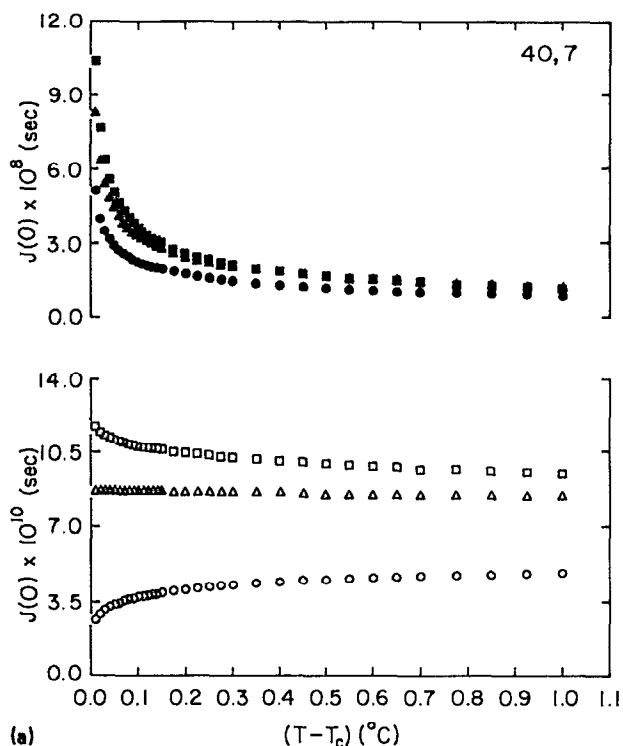
B. N–S_A transition

Unlike the N–I transition which is weakly first order, the N–S_A transition is believed to be second order for 4O,6 (Refs. 9–11) and 6OCB–8OCB.[12,13] Consistent with this, continuous changes in hyperfine splittings and g shifts, which measure the ordering of the spin probes, are observed. There are no discontinuous changes in the line positions (unlike the N–I transition) to provide an indication of a transition. On the other hand, the fact that density fluctuations which occur as smectic layers begin to form near T^* modulate the spin relaxation of the probe molecule provides a signature of the N–S_A transition. The linewidth parameters B and C are noted to diverge as the transition is approached.

Our analysis of the linewidth results at the N–S_A transition proceeds along the same lines as that for the N–I transition; the results are summarized in Table III.

1. Above the N–S_A transition

It is noted that $\sigma = -1/3$ in nearly all cases when the transition is approached from above. This includes the nematic side of the N–S_A transition as well as the smectic side of the S_A–RN transition. The $-1/3$ value for the exponent is rationalized in terms of the model (as discussed above) which treats fluctuations in spin-relaxation parameters as being coupled to density fluctuations which occur as the transition is approached from above. In Appendix C, calculations of the secular (and pseudosecular) spectral density are shown using experimental data (e.g., coherence lengths) appropriate to 6OCB–8OCB and 4O,7, the latter being taken as an approximation to 4O,6 (which like 4O,7 also exhibits a second-order N–S_A phase transition). It is clearly noted that for both liquid crystals $J(0)$ diverges as T approaches T_c [cf. Tables IV and V and Figs. 7(a) and 7(b)], whereas $J(\omega_a)$ does not diverge (e.g., see Fig. 8). However, for finite diffusion rates, the divergence in $J(0)$ is suppressed if we adopt model I, which allows for uniform averaging through a smectic layer (i.e., $q_s \neq 0$). (Thus critical exponents are very small, approaching zero.) On the other hand, in the other limit (model II) where probe diffusion through the smectic layer is significantly hindered (i.e., $q_s = 0$), but overall diffusion is not, then a substantial critical exponent σ is predict-
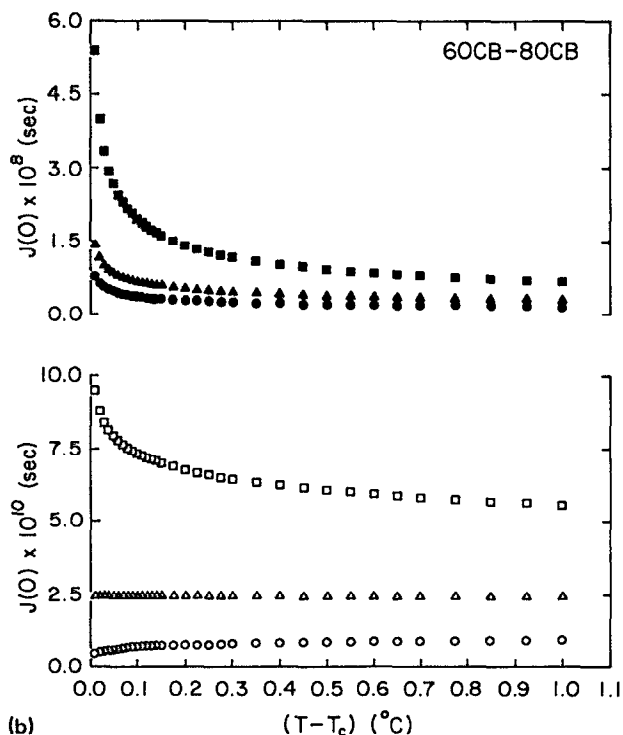
FIG. 7. Temperature dependence of secular spectral density $J(0)$ near the N–S_A transition, calculated using parameters appropriate to (a) 4O,7 (see Table IV) and (b) 6OCB–8OCB (see Table V). The cases shown here correspond to the following cases in Tables IV and V: (i) solid squares, case 3; open squares, case 7; (ii) solid triangles, case 4; open triangles, case 8; (iii) circles: similar to (ii), but with $x_\perp = x_\parallel = 1.0$.
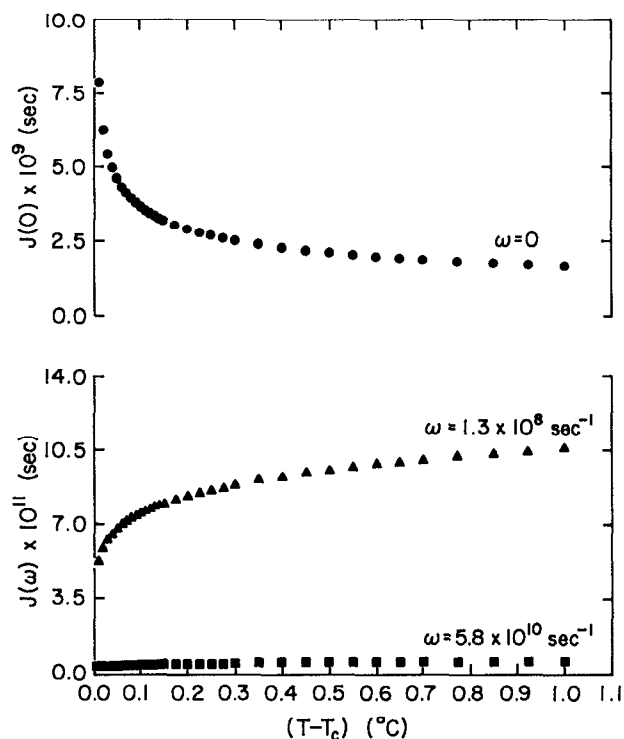
FIG. 8. Temperature dependence of spectral density $J(\omega)$ at frequencies corresponding to (i) circles, secular ($\omega = 0$); (ii) triangles, pseudosecular ($\omega \sim 1.3 \times 10^8$ s^{-1}); and (iii) squares, nonsecular ($\omega \sim 5.8 \times 10^{10}$ s^{-1}) terms. Parameters used are those of Table V, case 4, but with $x_\perp = x_\parallel = 1$. [Note that (i) and (ii) are rather insensitive to values of q_c, whereas case (iii) is very sensitive to q_c. For case (iii) only we show here the result $q_c = \infty$, since this provides the upper limit; finite q_c values lead to even smaller nonsecular $J(\omega)$.]

isotropic scaling, i.e., case 10). The experimental values of close to $-1/3$ would have to be rationalized in terms of some intermediate case between models I and II (but lying closer to model II) in which probe diffusion through the smectic layer is only partially hindered. This is perhaps closer to the situation studied deep in the smectic phase.[48]

2. Below the *N*–*S$_A$* transition

In most cases, no critical divergence is noted to occur when the N–S_A transition is approached from the S_A phase (except for P in 4O,6, as discussed below). The lack of a divergence from the S_A side of the transition is rationalized as likely due to the fact that only data significantly below T_{NA} (by at least 0.3 °C) could be utilized (cf. Sec. II D). Thus there would already be a finite Ψ_0 (cf. Appendix D), i.e., well-formed smectic layering, inducing the expulsion of the spin probe into the chain regions, so that the probe is no longer very sensitive to the fluctuations in Ψ. This is supported by the fact that the diverging linewidths in the nematic phase are approaching the smectic-A values. In the S_A phase, we have the full expulsion effect operative: i.e., the probe traverses the smectic layer, sampling the nonuniform distributions along the smectic layer which fully provides this new relaxation process.[48]

ed. Typical values (case 9 in Tables IV and V) are -0.54 for 4O,7 and -0.48 for 6OCB–8OCB utilizing the anisotropic exponents discussed in Appendixes B and C (but lowered values of -0.47 and -0.364, respectively, with Brochard's

However, a divergence in B and C at the S_A side of the NA transition for P in 4O,6 is observed. Similar, but qualitative divergences have been seen in the S_A phases of 4O,7, 6O,4, 7O,5.[49] Unlike PD-tempone and MOTA, the B and C values associated with P-probe do not exhibit a critical divergence as the NA transition is approached from the high-temperature phase.

One mechanism that could be involved in the divergences observed for P-probe would be fluctuations in S, the nematic order parameter, at the $N-S_A$ transition.

Unlike PD-tempone and MOTA, the P-probe in 4O,6 does not undergo expulsion at the NA transition, possibly due to its liquid-crystal-like structure.[26,47] This could explain why it does not exhibit any divergence on the nematic side of the transition. On the other hand, it could lead to this probe being sensitive to the fluctuations in smectic order as the NA transition is approached from below. (It would be of interest to study P-probe in 6OCB–8OCB since this spin probe is not well incorporated into the bilayers in this case.) The simple Landau–deGennes theory predicts that for an NA transition the magnitude of S is enhanced in the smectic phase, and it is related to Ψ as[2]

$$\Delta S = \tfrac{1}{2} C \chi |\Psi|^2, \qquad (39)$$

where S, Ψ, and C are, respectively, the nematic order parameter, the smectic order parameter, and the coupling coefficient between the two order parameters. χ is the nematic susceptibility. Thus, time-dependent critical fluctuations in $|\Psi|^2$ will cause fluctuations in S which may lead to a critical divergence in the B and C parameters for the probes that are not expelled into the hydrocarbon regions. Fluctuations in S are usually ignored in theories of *dynamics* at the $N-S_A$ transition, since it is regarded as largely saturated, but experiments[49,50] make clear that this is not so. However, it is easy to show that in the standard linearized theory, such coupling effects do not appear (cf. Appendix D). Nevertheless, such couplings may be expected to be important, but their analysis would require a more sophisticated theory which would allow for higher-order effects (see also Ref. 51).

One might ask what might be the influence of second sound on the dynamics of the spin probe as one decreases the temperature below T_{NS_A} (cf. Ref. 21 of Paper I). Second sound, which is a propagating compression mode of the smectic layers, requires well-formed smectic layers to be important (i.e., it becomes significant deep in the S_A phase). We expect that compression effects are much less significant for spin probes (like PD-tempone and MOTA) than their expulsion with the formation of smectic layers in the first place. In fact, as the spin probes are expelled to the alkyl chains, they should be less sensitive to second sound, since one would expect the effects of second sound to be pronounced primarily in the hard cores of the liquid-crystal molecules. However, it could be that larger spin probes such as P or CSL which are (usually) better incorporated into the layer structure and couple to the hard-core regions[22,26,27,45,47] would have their dynamics modulated, but past ESR studies of rotational dynamics in smectics do not appear to manifest such effects.[22,26,27,45,47]

3. Magnitude of the critical effects

We now wish to consider the order of magnitude of the critical effects at the $N-S_A$ transition. The actual anomalous portion of the linewidth depends on $(\Delta Q)^2 J(0)$ [cf. Eq. (32) and Refs. 20 and 21]. If we consider typical results for PD-tempone at the $N-S_A$ transition given in Table III, we find that the linewidth contribution of $(\Delta Q)^2 J(0)$ is of the order of 10 mG at $(T - T_c) = 1\,°C$ corresponding to $1.76 \times 10^5\,s^{-1}$ in angular frequency units.

A fluctuation ΔQ in the ESR frequencies of the order of $1.76 \times 10^7\,s^{-1}$ (i.e., 1 G) seems entirely reasonable to us. For example, for PD-tempone, this corresponds to a change of order parameter $S^{(p)}$ by an amount $\delta S^{(p)} \sim 0.05$ (i.e., the hyperfine shift as well as the g shift are of the order of a gauss when $S^{(p)}$ changes by this amount[27,28]). In fact, in the recent study of Gorcester, Rananavare, and Freed,[48] it was suggested that deep in the smectic phase $\delta S^{(p)} \sim 0.85$ for PD-tempone as it translates in the parallel direction through a single bilayer (this corresponds to a minimum value of $S^{(p)} \sim 0.0$ in the middle of the chain region and a maximum $S^{(p)} \sim 0.85$ with PD-tempone in the middle of the headgroup region). Thus, in the spirit of an order-of-magnitude estimate, $J(0) \sim 0.57 \times 10^{-9}\,s$ at $T - T_c = 1\,°C$ would be consistent with experiment and with this estimate of ΔQ. Examination of Tables IV and V [see also Figs. 7(a) and 7(b)] show that for model II ($q_s = 0$), typical values of $J(0)$ at $T - T_c = 1\,°C$ are of the order of $10^{-8}\,s$, and even for model I ($q_s \neq 0$), are of the order of $10^{-9}\,s$. These values are even greater than would appear to be needed to agree with experiment, i.e., even smaller fluctuations in ΔQ than estimated above could be consistent with the experimental results.

4. Further comments

When we compare results for PD-tempone in different liquid crystals as well as the results with different spin probes, we can make the following observations. The effects at the $N-S_A$ transition are greater for PD-tempone in 6OCB–8OCB than in 4O,6. This parallels the results at the $N-I$ transition, and we may suppose that it is again consistent with the higher ordering of PD-tempone in the former solvent, and also the greater change in ordering of PD-tempone in the S_A phase over its nematic value in 6OCB–8OCB. The results for MOTA also show a substantially greater effect in 6OCB–8OCB than in 4O,6, but as discussed in Sec. III the results in 6OCB–8OCB are statistically not so reliable. We may suppose that in the bilayer-forming liquid crystal (6OCB–8OCB) there is greater opportunity for fluctuations of the probes than in the monolayer case (4O,6), but this warrants further study. These comments, of course, refer to the magnitude of $(\Delta Q)^2$. [Note that theoretically we predict the greater effect in 4O,7 for $J(0)$, but given the great uncertainty in estimates of τ_m and M_v, for which no values are known in the two solvents, this is of little significance at present.]

Most surprising is the absence of any observable critical divergence at the $S_A - N$ transition. We are inclined to relate this to the strong but nonlinear dependence upon the smectic

order parameter Ψ of probe location within the smecticlike layering, plus the fact that we are not able to measure accurate linewidths to within less than about 0.3 °C (i.e., $t\sim9\times10^{-4}$) due to line-shape distortions (noted in Sec. II D and below). At this value of $T_c - T$ into the S_A phase, there is already a significant equilibrium $\Psi = \Psi_0$,[40] and one may suppose that this suppresses fluctuations in probe location due to fluctuations in Ψ about Ψ_0.

However, in the specific case of a reentrant nematic we do note in the case of PD-tempone a critical divergence on the S_A side of the S_A–RN transition and not on the RN side. This is the only statistically significant example of such an effect, and one would like to see it confirmed. (A weaker effect has been observed for MOTA; cf. Table III.) If it is true, then given that the $RN\rightarrow S_A$ transition is basically the same sort of transition as is the N–S_A transition,[12] it would, at first, appear surprising. However, given that our ESR studies of the probes are directly sensitive to the nematic order parameter, S, and only indirectly senstive to smectic order parameter Ψ (via such mechanisms as we have already discussed), then it is useful to note that as one crosses the N–S_A transitions *and* as one crosses the S_A–RN transition (i.e., as one reduces the temperature), then the nematic ordering consistently increases for PD-tempone.[22] One would have to suppose a greater sensitivity of the probe to fluctuations when it is more weakly ordered, although we have no precise mechanism to describe this.

5. Line-shape asymmetry

In addition to the behavior of the linewidths, an independent signature of the N–S_A transition is the observed line-shape distortions as the transition is approached from either side (cf. Sec. II D). As the N–S_A transition is approached from the S_A side, distortions in the smectic layers occur as the elastic constant B for the compression of the smectic layers approaches zero. The alignment of our samples in the S_A phase represents a complex interplay of wall alignment, their transmission by smectic layering forces (measured by the elastic constant B), and the magnetic field.[26,27] As the smectic energy for compression decreases, the overall alignment is affected, and is manifested as a "static distribution of directors." The overall line shape is thus distorted.[27] As the N–S_A transition is approached from the nematic side, the formation of transient smectic layers with an associated finite B may be expected to distort somewhat the magnetic-field alignment, thereby leading to line-shape distortions.

A crude but useful quantitative measure of the line-shape distortion is obtained from the line-shape asymmetry, which for a given hyperfine line is defined as the ratio of the first derivative lobe heights. Since the line-shape asymmetry depends strongly on the spectrometer tuning, in our experiments the central line was symmetrized at all temperatures, and the asymmetry ratios of the outer lines with respect to the central line were considered. The results for the behavior of the relative asymmetry of the low-field line, η, are shown in Fig. 9 for PD-tempone in 6OCB-8OCB, and the curves through the data points represent nonlinear least-squares fits
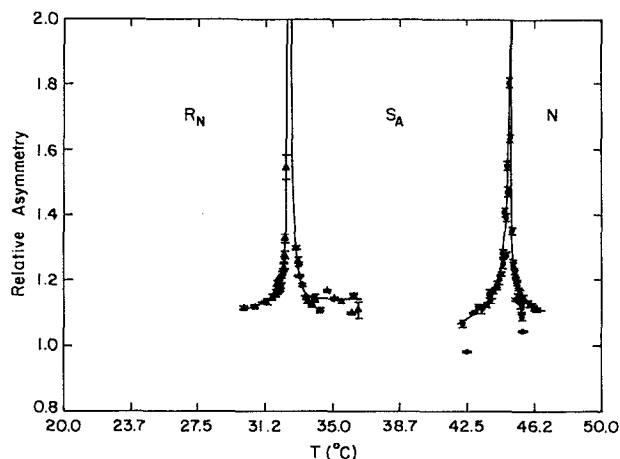

FIG. 9. Nonlinear least-squares analysis of the temperature dependence of the relative asymmetry of low-field line (with respect to central line) at N–S_A and S_A–R_N transitions for PD–tempone in 6OCB–8OCB.

to a model containing a constant background term Q and a divergent term $P\,|T - T_0|^y$:

$$\eta = Q + P\,|T - T_0|^y,$$

where T_0 is associated with the N–S_A transition temperature and y is a critical exponent. The usefulness of this fit lies in that it provides a measure of T_0 independent from that obtained from fitting the linewidths.

The results of our fits to the asymmetry data for PD-tempone in 4O,6 and 6OCB–8OCB are summarized in Tables VI(A) and VI(B). Even though the data is limited, our results show that while the "critical exponents" vary, the estimates of the critical temperature obtained on both sides of the transition are (with the exception of the S_A–RN transition in 6OCB–8OCB) very close, and are in good agreement with those determined from our nonlinear least-squares fits to the linewidths (see below). A theory of the critical behavior of the line-shape asymmetry has not yet been developed.

VI. CONCLUSIONS

A. The *N–I* transition

The quasicritical divergences in the ESR linewidths observed on both sides of the N–I transition are in all cases characterized by a critical exponent $\sigma = -1/2$. The results are fully consistent with the model of quasicritical fluctuations in the nematic order parameter which are sensed by the different spin probes that exhibit different degrees of probe ordering, and, as predicted, the more ordered the probe, the larger are the divergent contributions to the linewidths. These linewidth contributions are of the magnitude expected, given that key properties of the liquid crystals such as the relevant viscosities and force constants are not exactly known. The solvent-independent ratios of critical contributions to the ESR linewidths do show rather good agreement with theory especially in the case of PD-tempone, where the analysis has been extended to include the asymmetric ordering of this probe. This agreement involving the

TABLE VI. Nonlinear least-squares analysis of fits to the line-shape asymmetry parameter $\eta = P\,|T - T_0|^y + Q$ at $N \leftrightarrow S_A$ transitions.[a]

Transition	P	(A) PD–tempone in 6OCB–8OCB T_0	y	Q
S_A–N	$(1.85 \pm 0.01) \times 10^{-1}$	(45.00 ± 0.01)	(-0.72 ± 0.03)	$(9.84 \pm 0.05) \times 10^{-1}$
N–S_A	$(6.03 \pm 0.05) \times 10^{-2}$	(44.951 ± 0.003)	(-0.55 ± 0.01)	(1.060 ± 0.001)
RN–S_A	$(7.6 \pm 0.7) \times 10^{-2}$	(32.47 ± 0.01)	(-0.56 ± 0.01)	(1.063 ± 0.001)
S_A–RN	$(5.2 \pm 0.5) \times 10^{-2}$	(31.74 ± 0.71)	(-6.1 ± 0.5)	(1.14 ± 0.01)
Transition	P	(B) PD–tempone in 4O,6 T_0	y	Q
N–S_A	$(6.9 \pm 2.1) \times 10^{-3}$	(55.210 ± 0.005)	(-0.76 ± 0.04)	(1.071 ± 0.005)
S_A–N	$(2.9 \pm 1.8) \times 10^{-2}$	(55.205 ± 0.006)	(-0.99 ± 0.01)	(1.05 ± 0.01)

[a] η is defined as the ratio of the line-shape asymmetries of the low-field to middle-field lines.

sensitivity to such detail of probe ordering is, to our mind, a strong confirmation of the essential validity of the model. The principal discrepancy between experiment and theory is in the relative magnitudes of the quasicritical effects on either side of the N–I transition. Theory predicts a reduction by about a factor of $\sqrt{3}$ on the nematic side, but experimentally this is not generally the case. It is suspected that this matter may require a better understanding of how the probe molecules couple to the nematic order-parameter fluctuations on both sides of this weakly first-order transition.

B. The N–S_A transition

The N–S_A transition is second order for the liquid crystals studied as confirmed by the continuous change in ESR line positions across this transition. In general, critical divergences in the linewidths are observed on the nematic side of this transition for the weaker ordered probes, with a characteristic critical exponent $\sigma = -1/3$. These effects are typically weaker than those associated with the N–I transition, but have been carefully confirmed by the appropriate statistical tests. These observations are reasonably consistent with our proposed model of the dynamics of the probe molecules being coupled to the density fluctuations which exhibit critical fluctuations at this phase transition provided probe diffusion through the smecticlike layer is taken to be hindered. Some similar results are obtained on the high-temperature side of the S_A–RN transition. Detailed numerical calculations were performed which show that anisotropic critical exponents for the smectic correlation lengths and anisotropic diffusion both affect the predicted value of σ for these experiments. An analysis of the magnitude of the critical effects observed appears consistent with the probe order parameter (hence hyperfine shift and g shift) being modulated by the density fluctuations.

Below the N–S_A phase transition, such critical divergences are typically not observed. While this matter is not fully understood, it is suspected that the existence of a finite smectic order parameter, Ψ_0, acts to suppress any critically driven fluctuations in the behavior of the probes. It is be-

lieved that further understanding of these critical effects in the ESR spectra will require a better understanding of (1) to what extent nonlinear couplings can induce order-parameter fluctuations at the N–S_A transition, and (2) to what extent the critical density fluctuations affect translational diffusion of the probe molecules through the smectic layer. Also, spin-relaxation experiments less sensitive to cw line shapes at the phase transition (e.g., spin-echo and other time-domain experiments) should enable studies even closer to the phase transition.

APPENDIX A: ANISOTROPIC ORDER-PARAMETER FLUCTUATIONS AT THE NEMATIC–ISOTROPIC TRANSITION

In this section, the spectral densities for order-parameter fluctuations (OPF), which were used previously to calculate the critical contribution to the linewidth [Eq. (16)], are generalized to include anisotropic potentials, i.e., when the potential function $U(\Omega)$ for orientational order of the probe contains two parameters $\bar{\lambda}^{(p)}$ and $\bar{\rho}^{(p)}$, given by

$$U(\Omega)/k_b T = -\sum_N \{\bar{\lambda}^{(p)} \mathscr{D}^2_{0N}(\Omega) \mathscr{D}^2_{N0}(-\Psi)$$

$$+ \bar{\rho}^{(p)}[\mathscr{D}^2_{2N}(\Omega) \mathscr{D}^2_{N0}(-\Psi)$$

$$+ \mathscr{D}^2_{-2N}(\Omega) \mathscr{D}^2_{N0}(-\Psi)]\}. \tag{A1}$$

In Eq. (A1), Ω and Ψ refer, respectively, to the Euler angles of the probe molecule relative to the director, and the Euler angles for the director relative to the lab frame. The potential $U(\Omega)$ in Eq. (A1) is an extension of the one-parameter potential in Ref. 17. Thus, the calculations of the correlation functions for OPF at the N–I transition follow methods developed previously;[17] these are considered below for the isotropic and nematic sides of the transition. In both cases, it is

assumed that the fluctuations are in both the magnitude as well as the orientation of the potential.

1. Isotropic phase

Let $\Xi \to \Psi$ denote the instantaneous orientation of the director in the lab frame, and let $\Xi_{eq} \equiv \Psi_{eq}$ denote its equilibrium value. If $P_{eq,\Psi}(\Omega)$ denotes the equilibrium distribution function for molecular orientation Ω when the director orientation in the lab frame is Ψ, then following the definition of Freed,[17] we have

$$\Delta(\Psi,\Omega) \equiv P_{eq,\Psi}(\Omega) - P_{eq,\Psi_{eq}}(\Omega) \cong \Xi \Delta^{(1)}(\Omega). \quad (A2)$$

Following Freed,[17] for a two-parameter potential we have

$$\Xi \Delta^{(1)} = \frac{1}{8\pi^2} \left\{ \bar{\lambda}^{(p)} \sum_N \mathscr{D}^2_{0N}(\Omega)\mathscr{D}^2_{N0}(-\Psi) \right.$$

$$+ \bar{p}^{(p)} \sum_N [\mathscr{D}^2_{2N}(\Omega)\mathscr{D}^2_{N0}(-\Psi)$$

$$\left. + \mathscr{D}^2_{-2N}(\Omega)\mathscr{D}^2_{N0}(-\Psi)] \right\}. \quad (A3)$$

Equation (A3) holds for small $\bar{\lambda}^{(p)}$ and $\bar{p}^{(p)}$. Ξ (which is here equivalent to Ψ) specifies the instantaneous orientation of the director in the lab frame. One finds for small $\bar{\lambda}^{(p)}$ and $\bar{p}^{(p)}$ that

$$S^{(p)} \cong \tfrac{1}{5}\bar{\lambda}^{(p)}. \quad (A4)$$

In a similar fashion, we let

$$\tfrac{1}{5}\bar{p}^{(p)} \cong bS^{(p)}, \quad (A5)$$

where b is a scaling parameter chosen so that the ratio $\bar{p}^{(p)}/\bar{\lambda}^{(p)}$ is the same as in the nematic phase. Thus,

$$\Delta(\Psi,\Omega) \cong \frac{5S^{(p)}}{8\pi^2} \left\{ \sum_N \mathscr{D}^2_{0N}(\Omega)\mathscr{D}^2_{N0}(-\Psi) \right.$$

$$+ b \sum_N [\mathscr{D}^2_{2N}(\Omega)\mathscr{D}^2_{N0}(-\Psi)$$

$$\left. + \mathscr{D}^2_{-2N}(\Omega)\mathscr{D}^2_{N0}(-\Psi)] \right\}. \quad (A6)$$

Then Eqs. (2.33b) and (4.7′) in Ref. 17 require

$$\int d\Omega\, \mathscr{D}^{L*}_{K'M'}(\Omega)[\Xi\Delta^{(1)}]$$

$$= S^{(p)}\mathscr{D}^2_{M',0}(-\Psi)\delta_{L,2}[\delta_{K',0} + b(\delta_{K',\pm2})]$$

$$= (-1)^{M'}(S^{(p)}/S)Q_{-M'}\delta_{L,2}[\delta_{K',0} + b\delta_{K',\pm2}], \quad (A7)$$

where the last equality follows from the definition

$$Q_{M'} \equiv S\mathscr{D}^2_{0,M'}(\Psi) = S(-1)^{M'}\mathscr{D}^2_{-M',0}(-\Psi). \quad (A8)$$

Here, S is the order parameter for the liquid-crystal molecules. Similarly,

$$\int d\Omega\, \mathscr{D}^L_{KM}(\Omega)[\Xi\Delta^{(1)}]$$

$$= (-1)^{K-M}\int \mathscr{D}^{L*}_{-K-M}(\Omega)[\Omega\Delta^{(1)}]$$

$$= (-1)^K(S^{(p)}/S)Q_M\delta_{L,2}[\delta_{K,0} + b\delta_{K,\pm2}]. \quad (A9)$$

From these expressions, the required correlation function for OPF becomes [see Eq. (4.7′) in Ref. 17]

$$C^{(2)}_{M,-K,M',-K'}(t)$$

$$= (-1)^{M'}(S^{(p)}/S)^2\langle Q_{-M'}(0)Q_M(t)\rangle$$

$$\times [\delta_{K',0} + b\delta_{K',\pm2}][\delta_{K,0} + b\delta_{K,\pm2}], \quad (A10)$$

where [cf. Eq. C4 in Ref. 17]

$$\langle Q_{-M'}(0)Q_M(t)\rangle = \langle Q^*_M(0)Q_M(t)\rangle\delta_{M,M'}. \quad (A11)$$

This leads to the following expression for the spectral density [compare with Eq. (16)]:

$$J^{(2)}_{M,-K,M',-K'}(\omega) \cong \left(\frac{S^{(p)}_{NI}}{S_{NI}}\right)^2 \frac{k_b T}{4\sqrt{2}\pi} \left(\frac{\nu}{L^3\omega_\xi}\right)^{1/2}$$

$$\times \left\{ \frac{1}{1 + [1 + (\omega/\omega_\xi)^2]^{1/2}} \right\}^{1/2}$$

$$\times (\delta_{K,0} + b\delta_{K,\pm2})$$

$$\times (\delta_{K',0} + b\delta_{K',\pm2})\delta_{M,M'}. \quad (A12)$$

Note that $S^{(p)}_{NI}$ and S_{NI} refer to the ordering of the probe and the solvent, respectively, just at the N–I transition. Incorporation of the role of translational diffusion is by analogy to Eq. (18).

2. Nematic phase

The generalization of the expression for the correlation function for OPF at the nematic side of the N–I transition in Ref. 17 for a two-parameter ordering potential is performed similarly. [For convenience, we drop the superscripts on $\bar{\lambda}^{(p)}$ and $\bar{p}^{(p)}$ below and factor them as, e.g., $\bar{\lambda} = \bar{\lambda}_0 + \bar{\lambda}_1$ as defined below.] Consider,

$$\Delta(\Xi,\Omega) \equiv P_{eq,\Xi}(\Omega) - P_{eq,\Xi_{eq}}(\Omega)$$

$$= \frac{e^{Y(\Omega) + W(\Omega)}}{\int e^{Y(\Omega) + W(\Omega)}d\Omega} - \frac{e^{Y_0(\Omega) + W_0(\Omega)}}{\int e^{Y_0(\Omega) + W_0(\Omega)}d\Omega}, \quad (A13)$$

where

$$Y_0(\Omega) \equiv \bar{\lambda}_0 \mathscr{D}^2_{00}(\Omega), \quad (A14)$$

$$W_0(\Omega) = \bar{p}_0 [\mathscr{D}^2_{2,0}(\Omega) + \mathscr{D}^2_{-2,0}(\Omega)], \quad (A15)$$

$$Y(\Omega) \equiv Y_0(\Omega) + \bar{\lambda}_1 \mathscr{D}^2_{00}(\Omega - \Psi), \quad (A16)$$

$$W(\Omega) = W_0(\Omega) + \bar{p}_1 [\mathscr{D}^2_{2,0}(\Omega - \Psi) + \mathscr{D}^2_{-2,0}(\Omega - \Psi)]. \quad (A17)$$

Then,

$$\Xi\Delta^{(1)} = \left[\frac{1 + [Y(\Omega) - Y_d(\Omega)] + [W(\Omega) - W_0(\Omega)]}{Z + \int [Y(\Omega) - Y_0(\Omega)] + [W(\Omega) - W_0(\Omega)]e^{Y_0 + W_0}d\Omega} - \frac{1}{Z} \right] e^{Y_0(\Omega) + W_0(\Omega)}$$

$$\cong \frac{1}{Z}\{\bar{\lambda}_1 \mathscr{D}^2_{00}(\Omega - \Psi) + \bar{\rho}_1 [\mathscr{D}^2_{20}(\Omega - \Psi) + \mathscr{D}^2_{-20}(\Omega - \Psi)]$$

$$- \bar{\lambda}_1 \langle \mathscr{D}^2_{00}(\Omega - \Psi)\rangle + \bar{\rho}_1 [\langle \mathscr{D}^2_{20}(\Omega - \Psi)\rangle + \langle \mathscr{D}^2_{-20}(\Omega - \Psi)\rangle]\}, \tag{A18}$$

where $Z = \int e^{Y_0(\Omega) + W_0(\Omega)}d\Omega$. The last case is obtained by expanding the first denominator to lowest order. Therefore,

$$\Xi\Delta^{(1)} = P_{\mathrm{eq},\Psi_{\mathrm{eq}}}(\Omega)(5S^{(p)}) \left\{ \sum_N (\mathscr{D}^2_{0N}(\Omega) - \langle \mathscr{D}^2_{0N}(\Omega)\rangle_\Omega) \right.$$

$$\left. + b \sum_N [(\mathscr{D}^2_{2N}(\Omega) - \langle \mathscr{D}^2_{2N}(\Omega)\rangle_\Omega) + (\mathscr{D}^2_{2N}(\Omega) - \langle \mathscr{D}^2_{2N}(\Omega)\rangle_\Omega)] \right\} \mathscr{D}^2_{N0}(-\Psi). \tag{A19}$$

Now consider

$$\int d\Omega\, \mathscr{D}^L_{KM}(\Omega)[\Xi\Delta^{(1)}] = 5S^{(p)} \int d\Omega\, P_{\mathrm{eq},\Psi_{\mathrm{eq}}}(\Omega)\mathscr{D}^L_{KM}(\Omega) \left\{ \sum_N (\mathscr{D}^2_{0N}(\Omega) - \langle \mathscr{D}^2_{00}\rangle \delta_{N,0}) \right.$$

$$\left. + b \sum_N [(\mathscr{D}^2_{2N}(\Omega) - \langle \mathscr{D}^2_{20}\rangle \delta_{N,0}) + (\mathscr{D}^2_{-2N}(\Omega) - \langle \mathscr{D}^2_{-20}\rangle \delta_{N,0})] \right\} \mathscr{D}^2_{N,0}(-\Psi)$$

$$= 5S^{(p)}\{(\langle \mathscr{D}^L_{KM}(\Omega)\mathscr{D}^2_{0-M}(\Omega)\rangle_\Omega - \langle \mathscr{D}^L_{K0}\rangle_\Omega \langle \mathscr{D}^2_{00}\rangle_\Omega \delta_{M,0})$$

$$+ b [(\langle \mathscr{D}^L_{KM}(\Omega)\mathscr{D}^2_{2-M}(\Omega)\rangle_\Omega - \langle \mathscr{D}^L_{K0}\rangle_\Omega \langle \mathscr{D}^2_{20}\rangle_\Omega \delta_{M,0})$$

$$+ (\langle \mathscr{D}^L_{KM}(\Omega)\mathscr{D}^2_{-2-M}(\Omega)\rangle_\Omega - \langle \mathscr{D}^L_{K0}\rangle_\Omega \langle \mathscr{D}^2_{-20}\rangle_\Omega \delta_{M,0})]\}\mathscr{D}^2_{-M,0}(-\Psi)$$

$$= (-1)^K(S^{(p)}/S)5Q_M\{\kappa(K,0,M) + b [\kappa(K,-2,M) + \kappa(K,2,M)]\}, \tag{A20}$$

where, in the last equality in Eq. (A20), following the definition of Lin and Freed,[27] we have let

$$\kappa(K,K',M) \equiv \langle \mathscr{D}^{2*}_{KM}(\Omega)\mathscr{D}^2_{K'M}(\Omega)\rangle_\Omega - \langle \mathscr{D}^{2*}_{KM}\rangle_\Omega \langle \mathscr{D}^2_{K'M}\rangle_\Omega.$$

Similarly,

$$\int d\Omega\, \mathscr{D}^{L'*}_{K'M'}(\Omega)[\Xi\Delta^{(1)}] = (-1)^{M'}(S^{(p)}/S)5Q_{M'}\{\kappa(K',0,M') + b [\kappa(K',-2,M') + \kappa(K',2,M')]\}. \tag{A21}$$

In order to obtain the results in Eqs. (A20) and (A21), note that

$$\kappa(K,K',M) = (-1)^{K-M}[\langle \mathscr{D}^2_{-K-M}(\Omega)\mathscr{D}^2_{K'M}(\Omega)\rangle_\Omega - \langle \mathscr{D}^2_{-K-M}\rangle_\Omega \langle \mathscr{D}^2_{K'M}\rangle_\Omega].$$

However, from Eq. (B5) in Ref. 27, we have

$$\kappa(K,K',M) = \kappa(-K,-K',-M),$$

so that

$$\kappa(K,K',M) = (-1)^{K-M}[\langle \mathscr{D}^2_{KM}(\Omega)\mathscr{D}^2_{-K'-M}(\Omega)\rangle - \langle \mathscr{D}^2_{KM}\rangle_\Omega \langle \mathscr{D}^2_{-K'-M}\rangle_\Omega].$$

So the correlation function for OPF for a two-parameter potential [compare with Eq. (4.11) in Ref. 17] becomes

$$C^{(2)}_{M,-K,-K',M'}(t) = (-1)^K(S^{(p)}/S)^2 25\langle Q^*_M(0)Q_M(t)\rangle \delta_{M'M}\{\kappa(K,0,M) + b [\kappa(K,-2,M) + \kappa(K,2,M)]\}$$

$$\times \{\kappa(K',0,M') + b [\kappa(K',-2,M') + \kappa(K',2,M')]\}. \tag{A22}$$

The expression for the OPF spectral density thus becomes [with $\omega_{\bar{\xi}} = L_N/(\nu_N\bar{\xi}^2)$]:

$$J^{(2)}_{M,-K,M',-K'}(\omega) \cong \left(\frac{S^{(p)}_{NI}}{S_{NI}}\right)^2 \frac{k_b T}{4\sqrt{2}\pi} \left(\frac{\nu_N}{L^3_N \omega_\xi}\right)^{1/2} \left\{\frac{1}{1 + [1 + (\omega/\omega_\xi)^2]^{1/2}}\right\}^{1/2} \delta_{M'M}$$

$$\times 25\{\kappa(K,0,M) + b[\kappa(K,-2,M) + \kappa(K,2,M)]\}$$

$$\times \{\kappa(K',0,M') + b[\kappa(K',-2,M') + \kappa(K',2,M')]\}. \tag{A23}$$

In Eq. (A23), $S^{(p)}_{NI}$ and S_{NI} refer to the ordering of the probe and the solvent, respectively, just below the N–I transition. The function $\kappa(K,K',M)$ is tabulated in Table VII.

Equations (A12) and (A23) are appropriate in the case of a noncylindrically symmetric ordering potential, such as is typically noted for PD-tempone in liquid-crystal solvents. These equations, rather than those for the one-parameter potential shown in the text, were used for analyzing the PD-tempone linewidth data near the N–I transition.

3. Critical contributions to linewidth at the *N–I* transition

The line broadening due to OPF at the N–I transition, neglecting contributions from nonsecular terms, is given by

$$B_{\text{anom}} = -\frac{4\hbar\gamma_e^2}{\sqrt{6}\beta_e} \sum_K \sum_{K'} D_K F_{-K'} J^{(2)}_{K,K',0}(0) \tag{A24}$$

and

$$C_{\text{anom}} = \frac{\gamma_e^2}{24} \sum_K \sum_{K'} [8J^{(2)}_{K,K',0}(0) - 3J^{(2)}_{K,K',1}(\omega_a)], \tag{A25}$$

where the spectral densities $J^{(2)}_{K,K',M}(\omega)$ appearing in Eqs. (A24) and (A25) are given, at the isotropic and nematic

sides of the N–I transition, by Eqs. (A11) and (A23), respectively (with $M = M'$). The quantities D_K and F_K, which depend on the anisotropies of the hyperfine and g tensors, are defined elsewhere.[28] The expressions for k_B and k_C using these equations are found to be

$$k_B = -\frac{1}{3}\gamma_e B_0 \frac{1}{8\pi} \frac{k_b T\nu}{L^{3/2}a^{1/2}}$$

$$\times \left[\frac{1}{3}A_0 g_0 + \frac{2}{\sqrt{6}}(A_0 g_2 + A_2 g_0)b + 2A_2 g_2 b^2\right]$$

$$\times \left(\frac{S^{(p)}_{NI}}{S_{NI}}\right)^2 \tag{A26}$$

and

$$k_C = \frac{\gamma_e}{24} \frac{1}{8\pi} \frac{k_b T\nu N_C}{L^{3/2}a^{1/2}} \left[\frac{1}{3}A_0^2\right.$$

$$\left. + \frac{4}{\sqrt{6}}A_0 A_2 b + 2A_2^2 b^2\right]\left(\frac{S^{(p)}_{NI}}{S_{NI}}\right)^2 \tag{A27}$$

for the isotropic phase, which reduce to Eqs. (24) and (25) for $b = 0$. In the nematic phase, k_B and k_C are given by

$$k_B = -\frac{1}{3}\gamma_e^2 B_0 \frac{1}{8\pi} \frac{k_b T\nu_N}{L_N^{3/2}a^{1/2}\sqrt{3}} \left(\frac{S^{(p)}_{NI}}{S_{NI}}\right)^2$$

$$\times \left\{\frac{1}{3}A_0 g_0 F(0,0,0) + \frac{1}{\sqrt{6}}(A_0 g_2 + A_2 g_0)[F(2,0,0) + F(-2,0,0)]\right.$$

$$\left. + \frac{1}{2}A_2 g_2 [F(2,2,0) + F(2,-2,0) + F(-2,2,0) + F(-2,-2,0)]\right\} \tag{A28}$$

and

$$k_C = \frac{\gamma_e}{24} \frac{1}{8\pi} \frac{k_b T\nu_N}{L_N^{3/2}a^{1/2}\sqrt{3}} \left(\frac{S^{(p)}_{NI}}{S_{NI}}\right)^2 \left\{\frac{1}{3}A_0 A_0 [8F(0,0,0) - 3F(0,0,1)f(\omega_a)]\right.$$

$$+ \frac{1}{\sqrt{6}}A_0 A_2 [8F(0,-2,0) - 3F(0,-2,1)f(\omega_a) + 8F(0,2,0) - 3F(0,2,1)f(\omega_a)$$

$$+ 8F(2,0,0) - 3F(2,0,1)f(\omega_a) + 8F(-2,0,0) - 3F(-2,0,1)f(\omega_a)]$$

$$+ \frac{1}{2}A_2 A_2 [8F(2,-2,0) - 3F(2,-2,1)f(\omega_a) + 8F(2,2,0) - 3F(2,2,1)f(\omega_a)$$

$$\left. + 8F(-2,-2,0) - 3F(-2,-2,1)f(\omega_a) + 8F(-2,-2,0) - 3F(-2,-2,1)f(\omega_a)]\right\}. \tag{A29}$$

In the above equations, the following definitions have been used: $A_0 = (A_{xx} + A_{yy} - 2A_{zz})$, $A_2 = (A_{yy} - A_{xx})$, $g_0 = (2g_{zz} - g_{xx} - g_{yy})$, and $g_2 = (g_{xx} - g_{yy})$. $F(K,K',M)$ is defined as

$$F(K,K',M) \equiv 25\{\kappa(K,0,M) + b[\kappa(K,-2,M) + \kappa(K,2,M)]\}\{\kappa(K',0,M') + b[\kappa(K',-2,M') + \kappa(K',2,M')]\}. \tag{A30}$$

TABLE VII. Mean-square values of the rotation-matrix elements $\mathscr{D}^L_{KM}(\Omega)$ including cross terms for anisotropic ordering.

$\kappa(K,K',M)$[a]			
K	K'	M	Function of ordering tensor
0	0	0	$\frac{1}{5} + \frac{2}{7}\langle\mathscr{D}^2_{00}\rangle_\Omega + \frac{18}{35}\langle\mathscr{D}^4_{00}\rangle_\Omega - \langle\mathscr{D}^2_{00}\rangle^2_\Omega$
0	0	1	$\frac{1}{5} + \frac{1}{7}\langle\mathscr{D}^2_{00}\rangle_\Omega - \frac{12}{35}\langle\mathscr{D}^4_{00}\rangle_\Omega$
0	0	2	$\frac{1}{5} - \frac{2}{7}\langle\mathscr{D}^2_{00}\rangle_\Omega + \frac{3}{35}\langle\mathscr{D}^4_{00}\rangle_\Omega$
2	2	0	$\frac{1}{5} - \frac{2}{7}\langle\mathscr{D}^2_{00}\rangle_\Omega + \frac{3}{35}\langle\mathscr{D}^4_{00}\rangle_\Omega - |\langle\mathscr{D}^2_{20}\rangle_\Omega|^2$
2	2	1	$\frac{1}{5} - \frac{1}{7}\langle\mathscr{D}^2_{00}\rangle_\Omega - \frac{2}{35}\langle\mathscr{D}^4_{00}\rangle_\Omega$
2	2	2	$\frac{1}{5} + \frac{2}{7}\langle\mathscr{D}^2_{00}\rangle_\Omega + \frac{1}{70}\langle\mathscr{D}^4_{00}\rangle_\Omega$
2	0	0	$-\left(\frac{2}{7} + \langle\mathscr{D}^2_{00}\rangle_\Omega\right)\langle\mathscr{D}^2_{20}\rangle_\Omega + \frac{9}{7\sqrt{15}}\langle\mathscr{D}^4_{20}\rangle_\Omega$
2	0	1	$-\frac{1}{7}\langle\mathscr{D}^2_{20}\rangle_\Omega - 6\left(\frac{7}{\sqrt{15}}\right)\langle\mathscr{D}^4_{20}\rangle_\Omega$
2	-2	0	$\frac{6}{\sqrt{70}}\langle\mathscr{D}^4_{40}\rangle_\Omega$
2	-2	1	$-\frac{4}{\sqrt{70}}\langle\mathscr{D}^4_{40}\rangle_\Omega$
2	-2	2	$\frac{1}{\sqrt{70}}\langle\mathscr{D}^4_{40}\rangle_\Omega$

[a] $\kappa(K,K',M)$ is defined in Appendix A. Note that $\kappa(K,M) \equiv \kappa(K,K,M)$.

$F(K,K',M)$ can be calculated using Table VII. The entries not listed in Table VII can be obtained using the symmetries of the $\kappa(K,K',M)$:[27]

$$\kappa(K,K',M) = [\kappa(-K,-K',M)]^* = \kappa(K,K',-M)$$
$$= \kappa(-K,-K',-M) = \kappa(K',K,M). \quad \text{(A31)}$$

Equations (A26)–(A29) are modified for finite translational diffusion exactly as discussed in Sec. IV A [cf. Eqs. (16) and (27)].

APPENDIX B: DYNAMIC SCALING AT THE *N*–S_A TRANSITION

Paper I deals with the general formulation of spin relaxation due to order-parameter fluctuations at the *NA* transition based on the Landau model. The main drawback of the classical treatment is that the experimentally measured critical exponents for the coherence lengths at the *NA* transition are larger than 0.5, the mean-field value. Since the order parameters at the *NA* and the superfluid–normal-fluid transition are similar, one may expect a similar power law (2/3) for the correlation length for the former. However, not only do the measured exponents $v_\perp$ and $v_\parallel$ for $\xi_\perp$ and $\xi_\parallel$ often exceed the 2/3 value, but they are also found to be anisotropic, i.e., $v_\perp \neq v_\parallel$. The implication of these findings is that the dynamic scaling exponent x, used in paper I and by Brochard,[39] cannot be uniquely defined. Therefore, we provide a simple generalization to account for the anisotropy in $v_\perp$ and $v_\parallel$ and the associated exponents $x_\perp$ and $x_\parallel$.

(i) *Effect of anisotropic critical exponents $v_\perp$, $v_\parallel$.* The Landau–Khalatnikov relation for the relaxation of Ψ, the smectic order parameter, can be written as[52]

$$\gamma_3 \frac{\partial\Psi}{\partial t} = -\frac{\delta F}{\delta\Psi}, \quad \text{(B1)}$$

where γ_3 is the viscosity associated with the lateral slip of the smectic layers, and F is the Landau free energy. Equation (B1) is not rigorous because it neglects propagating effects which lead to "second sound" in the smectic phase. We ignore such effects, since they should not be important for our experiments as discussed in Ref. 21 of paper I and Sec. V B 2. The general form of the free-energy density which takes into account nonclassical values for the critical exponents β, γ is given by Kortan *et al.*[12] [note β is the critical exponent for $\Psi \sim (T - T_c)^\beta$]:

$$F = F_0 + \frac{1}{2}a(T - T_c)^\gamma|\Psi|^2 + \frac{1}{4}b(T - T_c)^{\gamma - 2\beta}|\Psi|^4$$
$$+ \frac{1}{2M_v}|\nabla_\parallel\Psi|^2 + \frac{1}{2M_T}|(\nabla_\perp + iq_0n_\perp)\Psi|^2 + F_{el}, \quad \text{(B2)}$$

where $M_v = A/\xi^2_\parallel$, $M_T = A/\xi^2_\perp$, $A = (1/2)a(T - T_c)^\gamma$, $B = (1/2)b(T - T_c)^{\gamma - 2\beta}$, and F_{el} relates to the nematic director (cf. Appendix D). Following standard procedures one may then obtain the expression for τ_q; Chen and Lubensky find[53]

$$\tau_q = \frac{2\gamma_3}{a(T - T_c)^\gamma(1 + q^2_\perp\xi^2_\perp + q^2_\parallel\xi^2_\parallel)}. \quad \text{(B3)}$$

τ_m, the q-independent decay rate for the smectic order parameter in Eq. (30), is then identified as

$$\tau_m = 2\gamma_3/a(T - T_c)^\gamma. \quad \text{(B4)}$$

An important difference in the Landau treatment vs the renormalization-group (RG) approach arises from the fact that whereas γ_3 does *not* exhibit a critical divergence in the former, the RG calculation of Hossain *et al.*[54] shows that

$$\gamma_3 \propto \xi_\perp^{-\epsilon/2 - 3(v_\parallel - v_\perp)/2v_\perp} \quad \text{(B5)}$$

where $\epsilon = 4 - d$. Thus, for the superfluid case one has $v = v_\perp = v_\parallel = 2/3$, $d = 3$, $\gamma = 2v = 4/3$. Hence,

$$\tau_m = \frac{2\gamma_3}{a(T - T_c)^\gamma} \propto \frac{\xi_\perp^{-1/2}}{a(T - T_c)^{4/3}} \propto \frac{1}{(T - T_c)^1}. \quad \text{(B6)}$$

Thus the power-law behavior of τ_m goes as $\sim t^{-1}$ [where t is the reduced temperature, $t \equiv (T - T_c)/T_c$] for the superfluid case. Brochard's analysis summarized in Eqs. (31) is consistent with this result. However, in general, it will depend on t as

$$\tau_m = \tau^0_m t^{(3/2v_\parallel - v_\perp - \gamma)} \propto t^\zeta, \quad \text{(B7)}$$

where $\zeta = (3/2)v_\parallel - v_\perp - \gamma$.

(ii) *Asymmetric variation of τ_q with $\xi_\perp$, $\xi_\parallel$.* Consider the more general expression, based on Eqs. (B3) and (B4), which assigns different exponents $x_\perp$, $x_\parallel$ [not equal to unity, in general, by analogy to Eqs. (29)] to $q_\perp\xi_\perp$ and $q_\parallel\xi_\parallel$, respectively, in order to satisfy dynamic scaling:

$$\tau_q = \frac{\tau_m}{1 + (q^2_\perp\xi^2_\perp)^{x_\perp} + (q^2_\parallel\xi^2_\parallel)^{x_\parallel}}. \quad \text{(B8)}$$

Equation (B8) is the generalization of Eq. (31); thus it is also to be regarded as a simple interpolation form. Substitution of Eq. (B7) in Eq. (B8) leads to

$$\frac{1}{\tau_q} = \frac{1}{\tau_m} + \frac{(q_\perp \xi_\perp)^{2x_\perp}}{\tau_m} + \frac{(q_\parallel \xi_\parallel)^{2x_\parallel}}{\tau_m}$$

$$= \frac{1}{\tau_m} + \frac{q_\perp^{2x_\perp}}{b_\perp} t^{-2x_\perp \nu_\perp - (3/2)\nu_\parallel + \nu_\perp + \gamma}$$

$$+ \frac{q_\parallel^{2x_\parallel}}{b_\parallel} t^{-2x_\parallel \nu_\parallel - (3/2)\nu_\parallel + \nu_\perp + \gamma}, \qquad \text{(B9)}$$

where

$$b_i = \frac{(\xi_i^0)^{2x_i}}{\tau_m^0}, \quad i = \perp, \parallel,$$

and $\xi_\perp = \xi_\perp^0 t^{-\nu_\perp}$, $\xi_\parallel = \xi_\parallel^0 t^{-\nu_\parallel}$.

At the second-order NA phase transition only τ_m diverges, i.e., the $q \to 0$ mode undergoes critical slowing down. The τ_q modes for $|q| > 0$ do not diverge, but become solely dependent on some power of q as $T \to T_{NA}$, hence the quantities such as $\xi_i^{2x_i}/\tau_m$ (where $i = \parallel$ or $\perp$) must be independent of reduced temperature t. These conditions may then be used to determine the dynamic scaling exponents $x_\parallel$ and $x_\perp$ as

$$x_\perp = \left(\frac{-\tfrac{3}{2}\nu_\parallel + \nu_\perp + \gamma}{2\nu_\perp} \right), \qquad \text{(B10)}$$

and

$$x_\parallel = \left(\frac{-\tfrac{3}{2}\nu_\parallel + \nu_\perp + \gamma}{2\nu_\parallel} \right). \qquad \text{(B11)}$$

These equations can be further simplified using the scaling relation noted by Pershan and co-workers:[55]

$$\gamma = \nu_\parallel + \nu_\perp. \qquad \text{(B12)}$$

Although there exists no theoretical explanation of Eq. (B12), most of the x-ray data on the NA transition are consistent with Eq. (B12).

In the case of a superfluid where $\nu_\perp = \nu_\parallel = 2/3$, and $\gamma = 1.32$,[39] we find from Eqs. (B10) and (B11) that $x_\perp = x_\parallel \doteq 3/4$ in accordance with Brochard's dynamic scaling result[40] [i.e., the result of Eqs. (31)]. However, it may be noted that more generally, $x_\perp \neq x_\parallel$; thus for 4O,7 at the N-S_A transition, where $\nu_\perp = 0.65$ and $\nu_\parallel = 0.78$, we obtain $x_\perp = 0.72$ and $x_\parallel = 0.60$. Given that $\nu_\parallel \neq \nu_\perp$, then a knowl-

edge of $\nu_\parallel$ and $\nu_\perp$ would allow a more accurate determination of the spectral densities in the critical region than that based on the assumption that $x_\parallel$ and $x_\perp$ are 3/4 or 1. Such calculations are discussed in Appendix C.

APPENDIX C: EFFECTS OF ANISOTROPY OF THE MEDIUM ON SPIN RELAXATION NEAR CRITICAL REGIONS

The spectral density due to smectic order fluctuations is given by[21]

$$J(\omega) = \int d^3q \, J_q(\omega)$$

$$= \frac{V}{(2\pi)^3} \text{Re} \int_0^\infty dt \, e^{-i\omega t} \int_0^{q_c} d^3q \, C_q(t), \qquad \text{(C1)}$$

where $J_q(\omega)$ is the spectral density due to the qth mode of fluctuation, which is described by the correlation function $C_q(t)$. The latter is given by

$$C_q(t) = \frac{1}{4} \left[\frac{1}{\alpha_{q-q_s}} e^{-(\tau_{q-q_s}^{-1} + Dq^2)t} \right]. \qquad \text{(C2)}$$

Using the relations [see Eqs. (29) and (30)],

$$\alpha_{q-q_s}^{-1} = \frac{k_b T}{2AV} \frac{1}{1 + q_\perp^2 \xi_\perp^2 + (q_\parallel - q_s)^2 \xi_\parallel^2} \qquad \text{(C3)}$$

and

$$\tau_{q-q_s} = \frac{\tau_m}{1 + (q_\perp^2 \xi_\perp^2)^{x_\perp} + [(q_\parallel - q_s)^2 \xi_\parallel^2]^{x_\parallel}}, \qquad \text{(C4)}$$

and utilizing cylindrical coordinates to represent the axial symmetry with respect to the director in the smectic phase, i.e., replacing $\int_0^{q_c} d^3q$ by $2\pi \int_{-q_{\parallel,c}}^{q_{\parallel,c}} dq_\parallel \int_0^{q_{\perp,c}} q_\perp dq_\perp$, we obtain

$$J(\omega) = \frac{V}{4(2\pi)^2} \text{Re} \int_{-q_{\parallel,c}}^{q_{\parallel,c}} dq_\parallel \int_0^{q_{\perp,c}} dq_\perp q_\perp$$

$$\times \left(\frac{1}{\alpha_{q-q_s}} \frac{1}{\tau_{q-q_s}^{-1} + Dq^2 + i\omega} \right), \qquad \text{(C5)}$$

where $Dq^2 \equiv D_\perp q_\perp^2 + D_\parallel q_\parallel^2$. On substituting Eq. (C4) into Eq. (C5), we have

$$J(\omega) = \text{Re} \frac{k_b T}{4(2\pi)^2 A} \int_{-q_{\parallel,c}}^{q_{\parallel,c}} dq_\parallel \int_0^{q_{\perp,c}} dq_\perp q_\perp f_{q_\parallel - q_s}$$

$$= \frac{k_b T \tau_m}{4(2\pi)^2 A} \int_{-q_{\parallel,c}}^{q_{\parallel,c}} dq_\parallel \int_0^{q_{\perp,c}} dq_\perp q_\perp$$

$$\times \left(\frac{1}{1 + q_\perp^2 \xi_\perp^2 + (q_\parallel - q_s)^2 \xi_\parallel^2} \frac{1 + (q_\perp^2 \xi_\perp^2)^{x_\perp} + [(q_\parallel - q_s)^2 \xi_\parallel^2]^{x_\parallel} + D_\perp \tau_m q_\perp^2 + D_\parallel \tau_m q_\parallel^2}{\omega^2 \tau_m^2 + \{1 + (q_\perp^2 \xi_\perp^2)^{x_\perp} + [(q_\parallel - q_s)^2 \xi_\parallel^2]^{x_\parallel} + D_\perp \tau_m q_\perp^2 + D_\parallel \tau_m q_\parallel^2\}^2} \right), \qquad \text{(C6)}$$

where

$$f_{q_\parallel - q_s} \equiv \frac{1}{1 + q_\perp^2 \xi_\perp^2 + (q_\parallel - q_s)^2 \xi_\parallel^2} \frac{\tau_m}{1 + (q_\perp^2 \xi_\perp^2)^{x_\perp} + [(q_\parallel - q_s)^2 \xi_\parallel^2]^{x_\parallel} + (i\omega + D_\perp q_\perp^2 + D_\parallel q_\parallel^2)\tau_m}. \qquad \text{(C7)}$$

In these equations, the temperature dependence of A, τ_m, $\xi_\perp$, and $\xi_\parallel$ are as given in Appendix B, and the other symbols have been defined previously. Experimental data for the critical exponents $\nu_\perp$, $\nu_\parallel$, and γ and coherence lengths $\xi_\perp^0$ and $\xi_\parallel^0$ (see Appendix B) are available for 4O,7 (Ref. 10) and 6OCB–8OCB.[12,56] Rough estimates from experiment exist for τ_m and its temperature dependence,[20,40(b)] whereas $M_v = (2A\xi_\parallel^2)^{-1}$ is estimated from an expression suggested by Chu and McMillan:[57] $M_v = 2\pi^2/5nkTd^2$, where n is the number of molecules per unit volume. The diffusion rates $D_\perp = 5.9 \times 10^{-7}$ cm²/s, $D_\parallel = 4.6 \times 10^{-7}$ cm²/s are based on those estimated from data for PD-tempone in $S2$ using an ESR dynamic imaging (ESR–DID) method.[46]

We provide in Tables IV and V (for 4O,7 and 6OCB–8OCB, respectively) the secular spectral densities $J(0) = k(T - T_c)^\sigma$ by giving the values of k and σ for the two types of models (cf. Sec. IV B and Refs. 20 and 21), i.e., finite q_s (cases 5 and 6) and $q_s = 0$ in Eq. (C6) (all other cases) for zero and finite diffusion for purposes of comparison. We also compare the results obtained utilizing anisotropic exponents (cf. Appendix B) with those obtained using Brochard's isotropic scaling and $x = 3/4$; the latter are the even cases in the table and the entries are in parentheses. In general, the effect of using $x = 3/4$ instead of $x = 1$ as in the analytic results summarized in Sec. IV B is to increase the exponent σ slightly (ca. 10%) and to slightly enhance the coefficient k. The use of anisotropic exponents leads, in general, to increased values of σ (this is consistently true for 6OCB–8OCB parameters). The most important difference between the two sets of parameters utilized lies in the much larger coherence lengths for the 6OCB–8OCB mixture than for 4O,7. This means that diffusional averaging over a smecticlike cluster would be less effective for the case 6OCB/8OCB. Overall, while trends are similar for the two liquid crystals and consistent with the two analytic expressions of Sec. IV B, there are systematic differences in exponents for the two sets.

We show in Figs. 7(a) and 7(b) typical graphs of $J(0)$ vs $T - T_c$ comparing the results for anisotropic exponents, with isotropic exponents and $x = 3/4$, and with isotropic exponents and $x = 1$, for the two models corresponding to $q_s = 0$ (upper figure) and q_s finite (lower figure). In Fig. 8, results are given for $\omega = 0$ (secular), $\omega \sim 10^8$ s^{-1} (pseudosecular), and $\omega \sim 10^{10}$ s^{-1} (nonsecular) spectral densities. These results clearly indicate that (1) in the range $T - T_c \leqslant 1$ °C, the pseudosecular and nonsecular spectral densities are insignificant compared to the secular; and (2) near T_c, only $J(0)$ diverges. This emphasizes the importance of $J(0)$ in assessing the critical contribution to relaxation near the phase transition.

APPENDIX D: FLUCTUATIONS IN THE NEMATIC ORDER PARAMETER AT THE N–S_A TRANSITION

Deep in the nematic phase it is usually assumed that the nematic order parameter S is saturated, so there are only fluctuations in the *orientation* of the director. Experiments

make it clear, however, that the magnitude of S is still not saturated even at the second-order N–S_A transitions. In fact, ESR studies have shed light on the importance of S in driving the N–S_A transition.[49,50] Here, we modify the usual analysis of the N–S_A transition[38,39,40,53] to include fluctuations in S. We necessarily only consider linearized fluctuations.[39,40] Thus, we shall consider nematic ordering deep in the nematic phase to be described by $S\hat{n}$, the product of the magnitude and its orientation. Then, fluctuations would be described by $\hat{n}\delta S + S\delta\hat{n}$. For the relevant contributions to the free energy, we take Eq. (B2) with

$$F_N = \tfrac{1}{2}K_1(\nabla\cdot\hat{n})^2 + \tilde{K}_2(\hat{n}\cdot\nabla\times\hat{n})^2 + \tilde{K}_3(\hat{n}\times\nabla\times\hat{n})^2, \quad (D1)$$

which is the usual director free energy with bend, splay, and twist force constants K_1, K_2, and K_3, and the tilda's mean that these force constants show a critical divergence at the N–S_A transition. Equation (D1) will take account of $S\delta\hat{n}$.

We now rewrite the terms in F [cf. Eq. (B2)] that explicitly or *implicitly* include S in the absence of fluctuations in S:

$$F_{S_A} = F_0 + A(T)|\Psi|^2 + \beta_0(T)|\Psi|^4 + \gamma_0|\Psi|^6 + \delta S^2/2\chi, \quad (D2)$$

where we have necessarily included the last term[20,49,50] involving the nematic susceptibility χ, with $\delta S \equiv S - S_0$ and S_0 is the equilibrium value of S in the nematic phase neglecting any coupling between S and $|\Psi|^2$. (We have also added a term in $|\Psi|^6$ required for stability in the first-order region, and we have let $\beta_0 = B/2$.) To introduce this coupling we now recognize that S is a monotonic function of T, i.e., $S = S(T)$, and then let $T = T(S)$, so we rewrite $A = A(S)$ and $\beta_0 = \beta_0(S)$. Now expand $A(S)$ in a Taylor's series around S_0:[49,50]

$$A(S) = A(S_0) + A'(S_0)\delta S + A''(S_0)(\delta S)^2 + \cdots. \quad (D3)$$

Therefore,

$$F_{S_A} = F_0 + A(S_0)|\Psi|^2 + \beta_0(S_0)|\Psi|^4 + \gamma_0|\Psi|^6$$
$$+ (\delta S)^2/2\chi(S_0) - C(S_0)\delta S|\Psi|^2$$
$$+ \frac{1}{2}D(\delta S)^2|\Psi|^2 + \cdots, \quad (D4)$$

where $C(S_0) = -A'(S_0)$ and is the nematic–smectic coupling term usually introduced in an *ad hoc* fashion. Also, $D(S_0) = A''(S_0)$. Invoking the constraint $(\partial F/\partial \delta S) = 0$ yields

$$\delta S = \frac{\chi(S_0)C(S_0)|\Psi|^2}{1 + \chi(S_0)D(S_0)|\Psi|^2}. \quad (D5)$$

In the limit $\chi D|\Psi|^2 \ll 1$, substitution of Eq. (D5) into Eq. (D4) leads to the form

$$F_{S_A} = F_0 + A(S_0)|\Psi|^2 + \beta(S_0)|\Psi|^4 + \gamma|\Psi|^6 + \cdots, \quad (D6)$$

where $\beta = \beta_0 - (1/2)C^2\chi$ and $\gamma = \gamma_0 + (1/2)D\chi^2C^2$.

Equation (D6), while formally the standard result, has been derived from Eq. (D2) to make explicit the important role of the nematic ordering, S, in driving the N–S_A transition as discussed previously.[49]

We now consider fluctuations about the mean. We follow the standard Landau–de Gennes approach by only keeping quadratic terms. The only new terms we consider here are those due to fluctuations in δS, whereas the fluctuations represented by $\delta \hat{n}$ are given elsewhere,[39,40] so we ignore them here for simplicity in presentation. Then from Eq. (D4),

$$F_{\text{fluct}} \cong (A + \tfrac{1}{4}D \,\overline{\delta S^2})(|\Psi|^2 - |\Psi_0|^2)$$
$$+ (1/2\chi + \tfrac{1}{4}D \,|\Psi_0|^2)(\delta S^2 - \overline{\delta S^2})$$
$$+ \frac{1}{2} \int d^3\mathbf{r}\, L(\nabla \delta S)^2 + \cdots, \qquad (D7)$$

where the equilibrium values are $|\Psi_0|^2 = -A/2\beta$ and $\overline{\delta S^2} = \chi^2 C^2 |\Psi_0|^4$, and we have added a force constant L for distortions in $\delta S(\mathbf{r})$. After Fourier analysis and considering only δS_q, we have, for its mean-square fluctuation:

$$\langle |\delta S_q|^2 \rangle = \frac{k_b T}{\chi^{-1} + D |\Psi_0|^2 + Lq^2}, \qquad (D8)$$

which is nondivergent (even for $q \to 0$) at the N–S_A transition due to χ^{-1}, but it would be suppressed somewhat below the transition by the finite $|\Psi_0|^2$. Also, the viscosity associated with these fluctuations should be regular. However, a higher-order theory for the N–S_A transition involving mode coupling between fluctuations in $|\Psi|^2$ and δS might be expected to lead to a divergent contribution in δS.

[1] *Introduction to Liquid Crystals*, edited by E. B. Priestley, P. J. Wojtowicz, and P. Sheng (Plenum, New York, 1974); H. Kelker and R. Hatz, *Handbook of Liquid Crystals* (Verlag Chemie, Weinheim, 1980).

[2] S. Chandrasekhar, *Liquid Crystals* (Cambridge University, New York, 1977); P. G. deGennes, *The Physics of Liquid Crystals* (Oxford University, New York, 1974); M. J. Stephen and J. S. Straley, Rev. Mod. Phys. **46**, 617 (1974).

[3] M. A. Anisimov, Mol. Cryst. Liq. Cryst. **162A**, 1 (1988).

[4] T. W. Stinson and J. D. Litster, Phys. Rev. Lett. **25**, 500 (1970); **30**, 688 (1973).

[5] H. J. Coles and M. S. Sefton, Mol. Cryst. Liq. Cryst. **4**, 123 (1987).

[6] R. Y. Dong, G. M. Richards, J. S. Lewis, E. Tomchuk, and E. Bock, Mol. Cryst. Liq. Cryst. **144**, 33 (1987).

[7] C. R. J. Counsell, J. W. Emsley, G. R. Luckhurst, D. L. Turner, and J. Charvolin, Mol. Phys. **52**, 499 (1984).

[8] T. M. Barbara, R. R. Vold, R. L. Vold, and M. E. Neubert, J. Chem. Phys. **82**, 1612 (1985).

[9] R. J. Birgeneau, C. W. Garland, G. B. Kasting, and B. M. Ocko, Phys. Rev. A **24**, 2624 (1981).

[10] C. W. Garland, M. Meichle, B. M. Ocko, A. R. Kortan, C. R. Safinya, L. J. Yu, J. D. Litster, and R. J. Birgeneau, Phys. Rev. A **27**, 3234 (1983).

[11] B. M. Ocko, A. R. Kortan, R. J. Birgeneau, and J. W. Goodby, J. Phys. (Paris) **45**, 113 (1984).

[12] A. R. Kortan, H. V. Kanel, R. J. Birgeneau, and J. D. Litster, Phys. Rev. Lett. **47**, 1206 (1981); A. R. Kortan, H. V. Kanel, R. J. Birgeneau, and J. D. Litster, J. Phys. (Paris) **45**, 529 (1984).

[13] K. J. Lushington, G. B. Kasting, and C. W. Garland, Phys. Rev. B **22**, 2569 (1980).

[14] D. Brisbin, R. J. deHoff, T. E. Lockhart, and D. L. Johnson, Phys. Rev. Lett. **43**, 1171 (1979).

[15] J. Thoen, S. Marynssen, and W. van Dael, Phys. Rev. Lett. **52**, 204 (1984).

[16] K. V. S. Rao, J. S. Hwang, and J. H. Freed, Phys. Rev. Lett. **37**, 515 (1976).

[17] J. H. Freed, J. Chem. Phys. **66**, 4183 (1977).

[18] B. Cabane and W. G. Clark, Phys. Rev. Lett. **25**, 91 (1970).

[19] P. G. deGennes, Solid State Commun. **10**, 753 (1972).

[20] S. A. Zager and J. H. Freed, Chem. Phys. Lett. **109**, 270 (1984).

[21] J. H. Freed, preceding article, J. Chem. Phys. **96**, 3901 (1992); hereafter referred to as paper I.

[22] A. Nayeem and J. H. Freed, J. Phys. Chem. **93**, 6539 (1989).

[23] P. E. Cladis, Mol. Cryst. Liq. Cryst. **67**, 177 (1981).

[24] J. S. Hwang, K. V. S. Rao, and J. H. Freed, J. Phys. Chem. **80**, 1490 (1976).

[25] S. A. Zager, Ph.D. dissertation, Cornell University, 1982 (unpublished).

[26] E. Meirovitch and J. H. Freed, J. Phys. Chem. **84**, 2459 (1980).

[27] W. J. Lin and J. H. Freed, J. Phys. Chem. **83**, 379 (1979).

[28] C. F. Polnaszek and J. H. Freed, J. Phys. Chem. **79**, 2283 (1975).

[29] M. P. Eastman, R. G. Kooser, M. R. Das, and J. H. Freed, J. Chem. Phys. **51**, 2690 (1969).

[30] J. H. Freed, in *Spin Labeling: Theory and Applications*, edited by L. J. Berliner (Academic, New York, 1976), Chap. 3.

[31] D. M. Bates and D. G. Watts, *Nonlinear Regression Analysis and its Applications* (McGraw-Hill, New York, 1988).

[32] P. R. Bevington, *Error Analysis and Data Reduction in the Physical Sciences* (McGraw-Hill, New York, 1961).

[33] The rotational correlation times are the inverse of the eigenvalues $\tau_{L,K}^{-1}$ of the diffusion operator for axially symmetric diffusion in an isotropic phase, and are given by $\tau_{L,K}^{-1} \equiv R_\perp L(L+1) + (R_\parallel - R_\perp)K^2$. The precise definition of τ_R thus depends on the values of L and K associated with the spectral density of interest; thus, for $L = 2$, $K = 0$, $\tau_R \equiv \tau_{2,0}^{-1}$.

[34] P. Pincus, Solid State Commun. **7**, 415 (1969).

[35] $\kappa(M,K) \equiv \int P_{eq}(\Omega)(|\mathscr{D}_{MK}^2|^2 - \langle \mathscr{D}_{00}^2(\Omega) \rangle^2 \delta_{K,0}\delta_{M,0})d\Omega$, where $P_{eq}(\Omega)$ is the probability distribution function for the molecule (spin probe) in the potential field of the liquid-crystal solvent.

[36] $N_c = 8 - 3J_{10}(\omega_a)/J_{00}(0)$.

[37] T. W. Stinson, J. D. Litster, and N. A. Clark, J. Phys. (Paris), Colloq. **33**, C1-169 (1972).

[38] T. C. Lubensky, J. Chim. Phys. **80**, 31 (1983).

[39] F. Brochard, J. Phys. (Paris) **34**, 411 (1973).

[40] (a) F. Jahnig and F. Brochard, J. Phys. (Paris) **35**, 301 (1974); (b) F. Brochard, *ibid.* **37**, C3-85 (1976).

[41] A. D. Lawrie and S. Sarbach, in *Phase Transition and Critical Phenomena*, edited by C. Domb and M. S. Green (Academic, New York, 1984), Vol. 8.

[42] B. M. Ocko, R. J. Birgeneau, J. D. Litster, and M. E. Neubert, Phys. Rev. Lett. **52**, 208 (1984).

[43] Note that this does not mean that the interlayer spacing goes to zero, but it is the mathematical limit in which we can obtain a simple analytical form for the spectral density.

[44] J. P. Hornak, D. J. Schneider, and J. H. Freed, J. Chem. Phys. **84**, 3387 (1986); J. P. Moscicki, Y. K. Shin, and J. H. Freed, in *EPR Imaging and In Vivo EPR*, edited by G. R. Eaton, S. R. Eaton, and K. Ohno (CRC, Boca Raton, 1991), Chap. 19.

[45] A. Nayeem, S. B. Rananavare, V. S. S. Sastry, and J. H. Freed, J. Chem. Phys. **91**, 6887 (1989).

[46] Y. K. Shin, J. Moscicki, and J. H. Freed, Biophys. J. **57**, 445 (1990); and (unpublished).

[47] E. Meirovitch, D. Igner, E. Igner, G. Moro, and J. H. Freed, J. Chem. Phys. **77**, 3915 (1982).

[48] J. P. Gorcester, S. B. Rananavare, and J. H. Freed, J. Chem. Phys. **90**, 5764 (1989).

[49] S. B. Rananavare, V. G. K. M. Pisipati, and J. H. Freed, Liq. Cryst. **3**, 957 (1988).

[50] S. B. Rananavare, V. G. K. M. Pisipati, and J. H. Freed, Chem. Phys. Lett. **140**, 255 (1987).

[51] Brochard (Ref. 39) has shown that the spectral density associated with director fluctuations diverges with the critical exponent of $-1/3$ (neglecting diffusion) as the NA transition is approached from the S_A phase when $\omega \ll \Psi_0^2 q_z^2 / 2M_t \gamma_c$. However, as already pointed out above and in Refs. 17 and 21, a director-fluctuation mechanism is inconsistent with observed divergences in both the B and C (as well as A) terms. Another feature of the S_A phase which should have relevance is the fact that the smectic compression elastic constant B tends to zero with exponent 0.4 [cf. M. Benzekri, J. P. Marcerou, H. T. Nguyen, and J. C. Rouillon, Phys. Rev. B **41**, 1932 (1990)], but we do not have a mechanism to offer whereby this couples to the molecular dynamics or other properties of P-probe.

[52] L. Landau and I. Khalatnikov, Dokl. Acad. Nauk. SSSR **96**, 469 (1954); L. Landau and L. Lifshitz, *Physical Kinetics* (Pergamon, Oxford, 1983).

[53] J. L. Chen and T. C. Lubensky, Phys. Rev. A **14**, 1202 (1976).

[54] K. A. Hossain, J. Swift, J. H. Chen, and T. C. Lubensky, Phys. Rev. B **19**, 432 (1979).

[55] K. K. Chan, M. Deutsch, B. M. Ocko, P. S. Pershan, and L. B. Sorensen, Phys. Rev. Lett. **54**, 920 (1985).

[56] Note that the error bars quoted here were not reported in Ref. 12, but are based on those reported in the similar liquid crystals 8CB, 8OCB, and CBOOA [J. D. Litster, J. Als-Nielsen, R. J. Birgeneau, S. S. Dana, D. Davidov, F. Garcia-Golding, M. Kaplan, C. R. Safinya, and R. Schaetzing, J. Phys. (Paris) Colloq. **40**, 339 (1979); D. Davidov, C. R. Safinya, M. Kaplan, S. S. Dana, R. Schaetzing, R. J. Birgeneau, and J. D. Litster, Phys. Rev. B **19**, 1657 (1979)].

[57] K. C. Chu and W. L. McMillan, Phys. Rev. A **11**, 1059 (1975).